

NASICON BASED MATERIALS FOR SODIUM – ION – CAPACITORS

M.Tech. Thesis

By

NEHA



**DEPARTMENT OF METALLURGICAL ENGINEERING
AND MATERIALS SCIENCE**

**INDIAN INSTITUTE OF TECHNOLOGY
INDORE**

MAY 2024

NASICON BASED MATERIALS FOR SODIUM – ION – CAPACITORS

A THESIS

*Submitted in partial fulfillment of the
Requirements for the award of the degree
of
Master of Technology*

by
NEHA



**DEPARTMENT OF METALLURGICAL
ENGINEERING AND MATERIALS SCIENCE
INDIAN INSTITUTE OF TECHNOLOGY
INDORE**

MAY 2024



INDIAN INSTITUTE OF TECHNOLOGY INDORE

CANDIDATE'S DECLARATION

I hereby certify that the work which is being presented in the thesis entitled **NASICON BASED MATERIALS FOR SODIUM ION CAPACITORS** in the partial fulfilment of the requirements for the award of the degree of **MASTER OF TECHNOLOGY** and submitted in the **DEPARTMENT OF METALLURGICAL ENGINEERING AND MATERIALS SCIENCE, Indian Institute of Technology Indore**, is an authentic record of my own work carried out during the period from July 2023 to June 2024 under the supervision of **Dr. Dharendra Kumar Rai, Associate Professor IIT Indore**.

The matter presented in this thesis has not been submitted by me for the award of any other degree of this or any other institute.

NeHa
29/05/24

Signature of the student with date

(NEHA)

This is to certify that the above statement made by the candidate is correct to the best of my/our knowledge.

Signature of the Supervisor of

(with date) 29/05/24.

(Dr. Dharendra Kumar Rai)

NEHA has successfully given her M.Tech. Oral Examination held on **May 29, 2024**.

Signature of Supervisor of M.Tech. thesis

Date: 29/05/24.

Convener, DPGC

Date: 29/05/24.

ACKNOWLEDGMENTS

This thesis marks the end of an eventful and exciting journey during which there were many people whom I would like to acknowledge for their encouragement and constant support. First and foremost, I would like to express my sincere gratitude to my thesis supervisor Dr. Dharendra Kumar Rai for his valuable guidance, moral support, sharing of scientific ideas, constructive instructions, and useful technical suggestions throughout my M.Tech. project. His mentorship and guidance helped me bring out this research smoothly within a short span of time.

I would like to thank the Head of Department, Metallurgical Engineering and Materials Science IIT Indore, for providing me with the facilities to carry out my research work. I am also grateful to all other faculty members of the Department of Metallurgical Engineering and Materials Science during my M.Tech. Course. It is my great pleasure to express my hearty and eternal gratitude towards all of you.

I want to express my deepest gratitude to my senior colleague, Dr. Sarathkumar Krishnan for their support, valuable advice, timely help, feedback, and comments throughout my project. He became my great mentor; he always had the greatest ideas during our studies.

I owe my deepest gratitude to my lab mates, Mr. Mayank, Ms. Sheetal, Mr. Khushwant, Ms. Suporna, and Mr. Govind for giving me much enthusiasm and encouragement by providing me with significant research information and sharing experience, which helped me a lot during my project work.

I would like to express my heartfelt thanks to my husband, Mr. Akshay Kaundal for his support, patience, and encouragement have been my constant source of strength. He has been providing me the emotional support I needed and always believing me.

Finally, I thank all my teachers, classmates, and friends who supported me a lot throughout my career. I would like to thank IIT

Indore for providing research facilities and the opportunity to pursue M.Tech. Degree. I express my utmost thanks to all who helped me in one or another way directly and indirectly in the successful completion of my project. I am extremely indebted to each and everybody who has been associated with my project at any stage.

DEDICATION

Every challenging work needs self-effort as well as the guidance of elders, especially those who are very close to our hearts. I would like to dedicate this thesis to my parents and my husband Mr. Hoshiar Singh, Mrs. Tripta Devi, and Mr. Akshay Kaundal for their endless support and for keeping my spirit up with all the innocence. This thesis is also dedicated to one of my mentor, Dr. Sarathkumar, who has accompanied me through every effort and thought of this thesis.

ABSTRACT

Sodium-ion hybrid capacitors (SICs) are a potential class of energy storage devices that combine the best features of high-power capacitors and high-energy batteries while making use of cheap and plentiful sodium resources. However, conventional SICs use organic electrolytes that are highly combustible and show safety hazards, which mandates alternate and safe capacitor systems. Generally, the performance of the SIC device mainly depends on the electrode and electrolyte materials. In this thesis, we focused on engineering electrodes and electrolytes through doping and using high-concentration electrolytes, respectively for sodium-ion capacitors in the environmentally benign aqueous media. The low-concentration electrolytes usually suffer from a low Electrochemical stability window (ESW) of 1.23 V and the strong electrode dissolution in aqueous electrolytes that are barriers to the high energy density and extended lifespan of SICs. Firstly, this thesis introduces the high-concentration electrolytes concept with the concentration ranges from 1-17m NaClO₄ for achieving high ESW in SICs. With an ESW of 3.8 V, the 17m (mol kg⁻¹) NaClO₄ electrolyte showed remarkable storage performance using NASICON-based polyanionic cathodes Na₃V₂(PO₄)₃ (NVP). Additionally, the electrolyte showed a significant reduction in vanadium dissolution and stable charge-storage performance in NVP after using 17m NaClO₄.

On the other hand, NVP suffers from low electronic conductivity which impedes its further utilization in electrochemical applications. Therefore, a simple doping strategy has been used to improve the electronic conductivity as well as protect the electrode from capacity decay during long-term cycling. Herein, the cerium (Ce) with different concentrations (x=0.02, 0.04, 0.06, and 0.1) is used as a dopant to improve the performance of the NVP electrodes. Based on synthesis optimization, the impact of Ce substitution on the structural features such as morphology and crystal structure is

investigated using physical characterization tools such as XRD, FTIR, SEM, TEM, and EDX. Also, the electrochemical performances of Ce-modified NVPs ($\text{Na}_3\text{V}_{2-x}\text{Ce}_x(\text{PO}_4)_3$, $x=0.02, 0.04, 0.06, \text{ and } 0.1$) are examined using cyclic voltammetry (CV), galvanostatic charge-discharge (GCD), and electrochemical impedance spectroscopy (EIS). Among the different $\text{Na}_3\text{V}_{2-x}\text{Ce}_x(\text{PO}_4)_3$ formulations, $\text{Na}_3\text{V}_{1.96}\text{Ce}_{0.04}(\text{PO}_4)_3$ exhibits the improved electrochemical performances. It provides a discharge capacity of 83.98 mAhg^{-1} at 0.2 Ag^{-1} and 33.11 mAh g^{-1} even at 5 Ag^{-1} , which shows good rate performance. The maximum energy density $54.033 \text{ Wh.kg}^{-1}$ of at a Pdof 0.05 kW.kg^{-1} and a maximum Power density of 4.74 kW.kg^{-1} at 31.33 Wh.kg^{-1} . The capacity retention of $\text{Na}_3\text{V}_{1.96}\text{Ce}_{0.04}(\text{PO}_4)_3$ remains greater than 98% even after 100 cycles at 5 A/g current density.

Such an excellent performance may be the rationale for higher ionic radii of Ce^{3+} (1.034 \AA) than V^{3+} (0.74 \AA) acts as a pillar in the NVP structure which will ease the Na^+ mobility. The doping of Ce^{3+} led to the formation of a CeO_2 conductive layer on the NVP which will be the reason for the enhanced conductivity due to the n-type semiconductor nature of the CeO_2 layer. Overall, for the first time, Ce-doping and high-concentration electrolyte in the NVP shows excellent performance towards aqueous sodium-ion capacitor, which opens new avenues of exploring NASICON electrodes for aqueous energy storage systems in practical applications.

TABLE OF CONTENT

| Title | Page No. |
|-----------------------------------|--------------|
| Acknowledgement | I |
| Dedication | III |
| Abstract | IV |
| List of figures | xi |
| List of tables | xii |
| List of Abbreviations | xiii |
| Nomenclature | xiv |
| Introduction | 1-12 |
| Introduction | 1-4 |
| Literature Review | 4-12 |
| Thesis objective and scope | 12 |
| Organization of thesis | 12 |
| Experimental Section | 13-25 |
| Chemicals | 13 |
| Synthesis of NVP | 14 |
| Synthesis of Ce-doped NVP | 14 |
| Synthesis of MXenes | 15 |
| Modification of working electrode | 16 |
| Modification of electrolyte | 17 |
| Electrochemical measurement | 18 |
| Device fabrication | 19 |
| Performance indicators | 19 |
| Result and Discussion | 20-36 |
| Physical characterization | 20-25 |
| XRD pattern of materials | 20 |
| XPS analysis of materials | 21 |
| FTIR spectra | 22 |
| FESEM result | 24 |
| TEM result | 25 |
| Electrochemical performance | 25-36 |
| Solvent Modification | 29 |
| Three electrode characterization | 32 |

| | |
|------------------------------------|--------------|
| Two electrode characterization | 36 |
| Conclusion and future scope | 37-38 |
| Conclusion | 37 |
| Future scope | 38 |
| Reference | 39-41 |

LIST OF FIGURES

- Fig.1 World total primary energy consumption by fuel in 2019.
- Fig.2 Classification of electrochemical energy storage device.
- Fig.3 Historical timeline for the development of supercapacitors.
- Fig.4(a) Schematic diagram about charge storage mechanism for Electrochemical double-layer capacitors supercapacitors.
- Fig.4(b) Schematic diagram about charge storage mechanism for Pseudo capacitors.
- Fig.4(c) Schematic diagram about charge storage mechanism for Hybrid ion capacitors.
- Fig.5 Ragone plot of energy storage device.
- Fig.6 Classification of electrode materials for electrochemical supercapacitors.
- Fig.7 Schematic diagram of the preparation process of $\text{Na}_3\text{V}_2(\text{PO}_4)_3$.
- Fig.8 Schematic diagram of the preparation process of Ce-doped NVP materials.
- Fig.9 Schematic diagram of the synthesis process of MXenes.
- Fig.10 Schematic diagram of the preparation process of a slurry of cathode material.
- Fig.11 Schematic diagram of the preparation process of a slurry of anode material.
- Fig.12 Schematic diagram of the preparation process of electrolyte.
- Fig.13 Fabrication of three-electrode Swagelok cell.
- Fig.14 Fabrication of coin cell.
- Fig.15 XRD patterns of Ce- doped NVP.
- Fig.16 XPS patterns of Ce- doped NVP.
- Fig.17 FTIR spectra of Ce-doped NVP materials.
- Fig.18 FESEM image of Ce-doped NVP materials.
- Fig.19 EDX spectra and Elemental mapping of Ce-doped NVP materials.
- Fig.20 TEM, and HRTEM pattern of Ce- 4 NVP materials.
- Fig.21 Combine electrochemical performances of NVP for different concentration of electrolytes.
- Fig.22 CV profiles of NVP with different concentrations of electrolytes.
- Fig.23 GCD plots of the NVP with different concentrations of electrolytes.
-

| | |
|-----------|---|
| Fig.24(a) | Digital picture of Separator after cycling. |
| Fig.24(b) | Cyclic performance of NVP with 1m and 17m concentrations of NaClO ₄ electrolyte at 5A/g current density. |
| Fig.25 | Combine electrochemical performances of the Ce-doped NVP materials for three electrode characterization. |
| Fig.26 | CV profiles of the Ce-doped NVP materials samples for three electrode characterization. |
| Fig.27 | GCD plots for Ce-doped NVP materials samples for three electrode characterization. |
| Fig.28 | EIS spectra of the Ce-doped NVP materials samples for three electrode characterization. |
| Fig.29 | Combine electrochemical performances of the Ce-doped NVP materials for two electrode characterization. |
| Fig.30 | CV profiles for full cell of the Ce-doped NVP materials samples for two electrode characterization. |
| Fig.31 | GCD profiles for the full cell of the Ce-doped NVP materials samples for two electrode characterization. |
| Fig.32 | EIS spectra of the Ce-doped NVP materials for two electrode characterization. |
| Fig.33 | Rate performance of Ce-doped NVP materials material. |
| Fig.34 | Cyclic performance of Ce-doped NVP materials material. |

LIST OF TABLES

- Table 1. Comparison between Lithium based, and Sodium based energy storage systems.
- Table 2. Comparison between Aqueous and organic electrolytes.
- Table 3. Variation in the potential window of NVP material with different concentrations of electrolytes.
-

LIST OF ABBREVIATIONS

| | |
|-------|--|
| HICs | Hybrid ion capacitors |
| SICs | Sodium-ion hybrid capacitors |
| XRD | X-ray Diffraction |
| P-XRD | Powder X-ray diffraction |
| EDLC | Electric double-layer capacitance |
| LSV | Linear sweep voltammetry |
| ESW | Electrochemical stability window |
| CV | Cyclic voltammetry |
| GCD | Galvanostatic charge-discharge |
| EIS | Electrochemical impedance spectroscopy |
| PTFE | Polytetrafluoroethylene |
| WIS | Water-in-salt |
| SIW | Salt-in- water |
| PVDF | Polyvinylidene fluoride |
| P_d | Power density |
| CNTs | Carbon nanotubes |
| DOE | Department of Energy |
| E_d | Energy density |

NOMENCLATURE

| S. No. | Symbol | Meaning |
|--------|----------|---------------|
| 1 | A | Alpha |
| 2 | β | Beta |
| 3 | m | Molality |
| 4 | μ | Micro |
| 5 | M | Molar |
| 6 | θ | Bragg's angle |
| 7 | Na | Sodium |
| 8 | V | Vanadium |
| 9 | Ce | Cerium |
| 10 | P | Phosphorus |
| 11 | O | Oxygen |
| 12 | x | Concentration |

Chapter 1

Introduction

1.1 Introduction

Energy plays a crucial role in our contemporary lifestyle. However, our conventional method of generating electricity, primarily through the combustion of fossil fuels such as coal and oil, has serious ramifications. It contributes to global warming and irreversible climate change.

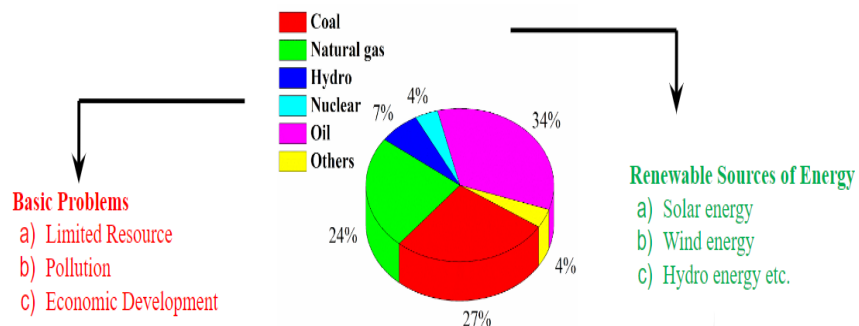


Fig. 1. World total primary energy consumption by fuel in 2019

To meet the demands of this sustainable world, electrical energy has been produced using renewable resources like tidal, solar, or wind energy [1]. This necessitates the exploration of cleaner energy production methods, harnessing the power features, which include excellent reversibility, high power density, and cycling stability. From all forms of energy storage technologies, batteries, and supercapacitors are a class of important and promising options. World total primary energy consumption by fuel in 2019 shown in **Fig. 1**.

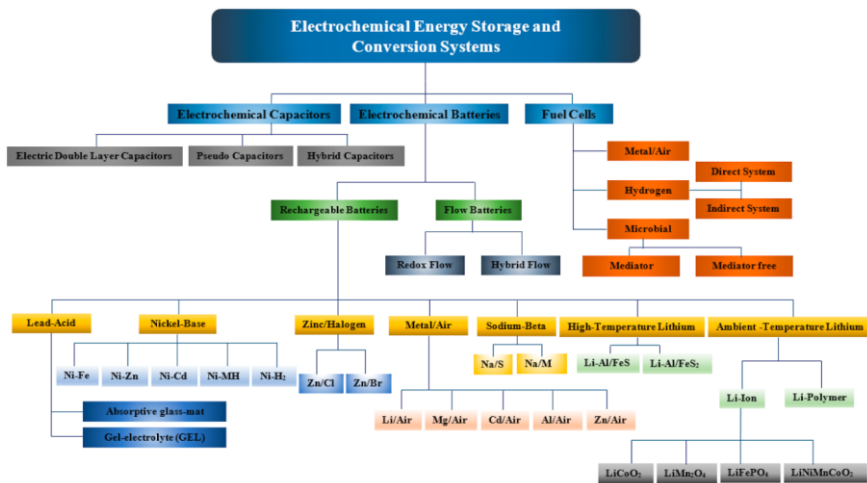


Fig. 2. Classification of electrochemical energy storage device.

The battery is an electrochemical device made up of external connectors and one or more electrochemical cells. They provide electricity for a variety of gadgets, including cell phones, laptops, and electric cars [2]. Although batteries have a large capacity to store electricity, it can take these gadgets up to several hours to fully charge. There are also various risks associated with their use such as leakage of corrosive chemicals, ingestion of battery, and use of toxic material for electrodes and electrolytes like lead, mercury, and cadmium metals. A capacitance is an electrochemical storage device that stores a sufficient amount of energy and charges almost at an instant period of time. Supercapacitors and batteries behave differently because they have different energy storage systems.

Redox reactions in the battery, which involve the transfer of electrons, store energy and produce increased energy density but decreased cyclic stability and power density. Supercapacitors have low energy density but render high Power density and long cyclic stability because energy is electrostatically stored in them through the formation of an electric double layer.

Unfortunately, despite intensive research efforts, neither the battery nor the supercapacitor has all three characteristics (energy density, power density, and cyclic stability independently [3]. Classification of electrochemical energy storage device shown in **Fig. 2.** Classification of electrochemical energy storage device

Using a combination of batteries and supercapacitors is one of the more promising ways to achieve the necessary features. This combination gave rise to a new platform of energy storage devices called hybrid ion capacitors. To support high power density and long cyclability, the HSCs constitute one battery-type electrode and one supercapacitor-type electrode. Various nanostructured materials are investigated to favor HSC electrode materials, including carbon-based materials, sulphides, and metal oxides. MXenes, and polyanion. Among these, polyanions have drawn a lot of attention for use in HSC devices as battery-type electrodes. It is mostly because of their unique characteristics like elevated Na^+ long cyclic life made possible by ion diffusivity, minimal lattice stress during Na^+ de-insertion, a large operating potential window, and increased structural and thermal stability.

NASICON have a general formula of $\text{A}_x\text{MM}'(\text{EO}_4)_3$, where A holds occupancy by alkali ions such as Li, Na, and K, or alkaline earth ions such as Mg and Ca, and M or M' sites are occupied by di, tri, tetra, and Pentavalent transition metal ions like Zn, Co, Ni, Mn, Fe, Sc, V, Ti, Zr, Sc, Mn, Nb and In for balancing the charge suitably, E is S, P, Si and As (Non-Metallic element) and $x=1-4$ [4]. The crystal structure may be rhombohedral, monoclinic, triclinic, or orthorhombic, depending on the composition. The $\text{M}(\text{M}')\text{O}_6$ octahedra and the EO_4 tetrahedra share common corners of a three-dimensional stiff framework that forms the rhombohedral structure. Corner-sharing oxygen ions bind two MO_6 octahedra and three EO_4 tetrahedra to produce highly covalently bound "lantern" structural units $[\text{M}_2(\text{EO}_4)_3]^{3-}$, which make up the NASICON framework. Na^+ ions A in $\text{A}_x\text{MM}'(\text{EO}_4)_3$ are dispersed at two separate interstitial sites such as N_1 and N_2 , the lantern units are arranged in a c-axis stack, and two separate interstitial sites contain the distribution of Na^+ ions in $\text{A}_x\text{MM}'(\text{EO}_4)_3$. These lantern units are arranged in a c-axis stack, and two separate interstitial sites contain the distribution of Na^+ ions in $\text{A}_x\text{MM}'(\text{EO}_4)_3$. Along the hexagonal c-axis, the octahedral N_1 sites is 6b share faces with two adjacent MO_6

octahedra. Fewer mobile Na^+ ions occupy these single sites per formula unit. Conversely, between the two EO_4 tetrahedra, there are three big N_2 sites per formula unit is $18e$ with eightfold coordination, which are filled by two mobile sodium ions.

As the coordinated oxygen atoms tightly bond with the sodium, Na^+ ions at N_1 sites, it is generally acknowledged that only sodium ions at N_2 sites are more readily removed or inserted for electrochemical action. NASICON often crystallizes with a thermally stable rhombohedral structure. Within this structure, the sodium ions go from one site to another via a hexagonal bottleneck area created by three XO_4 tetrahedra and three MO_6 octahedra sharing a corner. The rhombohedral phase is reversibly transformed to monoclinic distortion at high temperatures for selected compounds in the NASICON family (where $\text{A} = \text{Li}^+$, Na^+ , and $\text{M} = \text{Cr}$, Fe , Zr).

NASICON has poor electronic conductivity $10^{-12} \text{ S.cm}^{-1}$, which influences the rate capability and specific capacity. Various efforts have been undertaken to enhance its electronic conductivity, such as the application of carbon coatings and the doping of transition metals such as V, Mn, Ti, Cu, Cr and non-metallic elements such as F, S, P into NASICON, aimed at modifying their crystal and electronic structures to achieve the desired high-rate performance. Materials based on vanadium have the potential to be used as sodium ion hybrid capacitor electrode materials, especially in organic electrolytes. But vanadium's inevitable breakdown in aqueous electrolytes frequently leaves their aqueous phase counterparts with inadequate durability. Lower energy density resulting from the limited ESW created by water degradation in aqueous electrolytes exacerbates this problem.

High-concentration NaClO_4 electrolytes are added to overcome these difficulties by extending the ESW in the aqueous phase and enhancing durability. NVP shows good electrochemical behaviour hence it is a good material for energy storage devices. In addition to that, it has good chemical stability and is available in a

low-cost and non-toxic material [5]. It also has low electronic conductivity previous work shows that carbon coating, and doping of transition elements and non-metallic elements in NASICON-based material not only solves this problem but also improves the cycling performance.

In this thesis, we have synthesized the material for the Sodium ion hybrid capacitor, for playing the EDLC role we took carbonaceous material, and for doing redox reactions NASICON-based material was taken. We synthesize NASICON material by using the rheological phase reaction method. We have worked on the problem of metal dissolution and poor electronic conductivity of vanadium based NASICON material which is used as one of the best cathode materials in supercapacitors and batteries [6]. In aqueous electrolytes, there is very little research. Vanadium-based NASICON material shines like a luminary in the world of energy storage. It has high conductivity, excellent stability, and remarkable durability. Using vanadium in NASICON is a big deal because it means we can make better energy storage devices that last longer and work more efficiently.

1.2 Literature Review

1.2.1 The development of the supercapacitor technology:

Supercapacitors also termed 'electrochemical capacitors' or 'ultracapacitors' are a new variety for energy storage and conversion devices. Supercapacitors' origins can be traced to the discovery of charge storage mechanisms, the first of which is credited to German and Dutch scientists in 1745–1746 and is known as the Leyden jar [2]. It served as the prototype for the electric double-layer concept and stored static charge at the electrode interface by combining two metal foils with water, a conducting medium, in a glass jar. The first electric double of wind, solar, and ocean tides. Nevertheless, these resources cannot consistently provide energy, unlike fossil fuels due to their intermittent nature. To ensure the reliability of these clean energy sources, effective electrochemical energy storage solutions are essential. Supercapacitors have been the subject of extensive research because of their intriguing e-layer model, created by Von Helmholtz in 1853, which served as the foundation for the development of the current theory of electric double-layer capacitance (EDLC) in the late 19th and early 20th centuries. In 1954, H.I. Becker received the first patent for an electrochemical capacitor. Historical development over time is shown in **Fig.3**. The invention described an energy storage system that used porous carbon electrodes submerged in an aqueous electrolyte to store electric energy at the interfacial electric double layer. The "Super-Capacitor," as it was dubbed by NEC, was the first electrochemical capacitor to be commercialized in 1978. It was also the first to be used as a backup power source for CMOS memories and clock chips in electronics, a crucial use even today. With the development of the pseudo-capacitor in 1971, Faradaic techniques for energy storage were made possible. This provided a fresh method for boosting the charge-storage capacity of electrochemical capacitors and sparked several initiatives aimed at enhancing their performance. To meet the energy needs of electric and hybrid

vehicles, Maxwell Technologies and the U.S. Department of Energy (DOE) worked together to develop high-performance supercapacitors. The DOE started funding supercapacitor research for electric vehicles in 1989. Subsequently, a diverse range of supercapacitors, such as asymmetric supercapacitors, pseudo-capacitors, and EDLCs, have become accessible, each possessing unique features. Supercapacitor research has grown significantly and steadily since 2000 in response to the growing demand for extensive energy storage devices that are safe, reliable, and render high power.

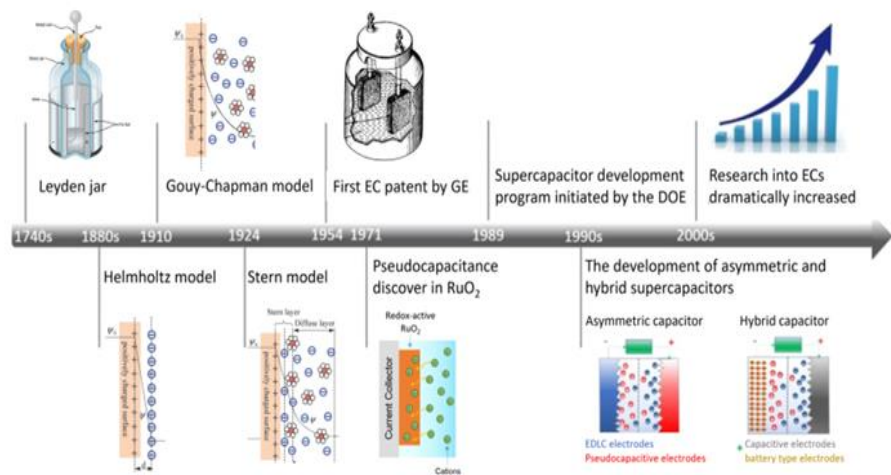


Fig. 3. Historical timeline for the development of supercapacitors [7].

1.2.2 Principles of energy storage in supercapacitors:

Depending on the different energy storage mechanisms, [8] Supercapacitors are classified into two types.

1. EDLC and
2. Pseudo-capacitor.

1.2.2.1 Electrochemical double-layer capacitors:

Similar to traditional capacitors, the ionic conducting electrolyte medium and electronic conducting electrode material form an interface that separates charges resulting in energy storage in an EDLC. Due to an electrostatic attraction, charges are stored by the adsorption of ions on the surface of the electrode from the

electrolyte for which another layer of charge is adhered on the surface, making double layers of ions, calling it a double-layer capacitor.

No charges are moving from the electrode to the electrolyte however, this interface's capacitance is referred to as the double layer capacitance holding an electrostatic charge storage mechanism [8]. EDLC electrode materials require a high surface area like 'activated carbon' known widely, high power density, excellent specific capacitance, and high conductivity. EDLCs constitute two carbon-based electrodes, an electrolyte, and a separator. While positive and negative ions are being moved to the electrode surfaces and separated from the bulk electrolyte, electrons are being forwarded from the positive electrode to the negative electrode via external power sources during the charge. Ions are released from the electrode surface and returned to the bulk of the electrolyte during the discharge, which involves the movement of electrons from the negative electrode to the positive electrode through the load.

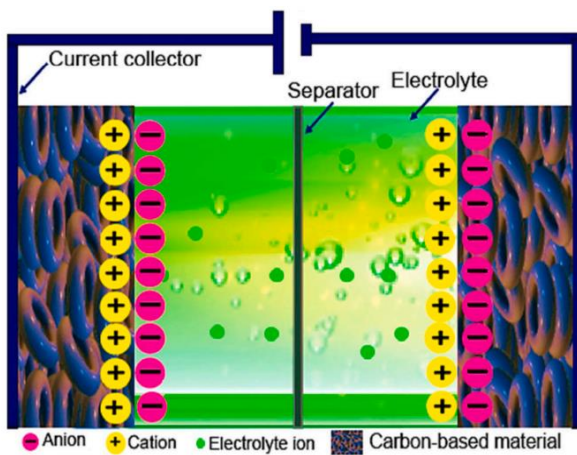


Fig. 4(a) Schematic diagram about charge storage mechanism for Electrochemical double-layer capacitors supercapacitors [8].

1.2.2.2 Pseudocapacitors:

Compared to EDLC, the mechanism of energy storage in pseudo capacitors is more complex. Unlike EDLC, the charges are stored in the pseudo-capacitor through redox reactions. Fast and reversible

oxidation and reduction reactions occur at the electrode-electrolyte interface on the surface as well as in the bulk of the electrode. Pseudo-capacitors render a very high capacitance value compared to EDLC because of the additional charge transferred but have less cycle life due to faradaic reactions. Generally, conductive polymers and metal oxide are used as pseudo-capacitors.

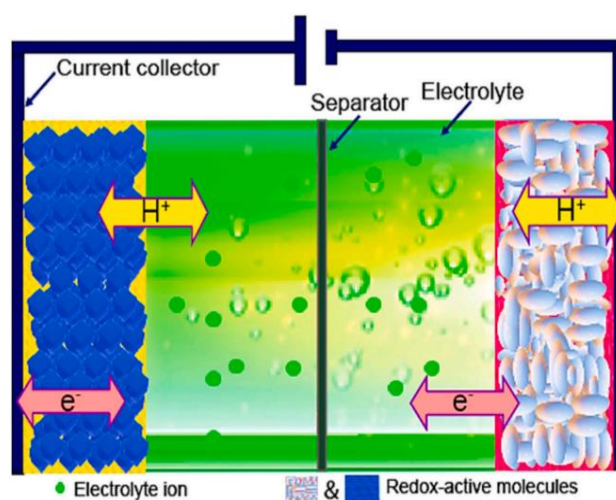


Fig. 4(b). Schematic diagram about charge storage mechanism for Pseudo capacitors [8].

1.2.2.3 Hybrid ion capacitors:

The ideal energy storage device would combine the strengths of both the battery and supercapacitor, offering high energy capacity, rapid discharge, and longevity. Recently, the development of HICs, which integrate the favourable attributes of batteries and supercapacitors, has attracted particular attention. HICs comprise an energy-retentive component and a rapid discharge component, offering a holistic solution to energy storage requirements [9]. Among the different HICs, the hybrid Li-ion capacitors (LIC), have significant development, but they suffer from relatively high costs due to their reliance on lithium, which is not abundantly available. To address this limitation, researchers are exploring an alternative solution known as SICs. Sodium, being more abundant than lithium and having a comparable electrochemical potential $E^{\circ} \text{Li} = -3.04 \text{ V}$, $E^{\circ} \text{Na} = -2.71 \text{ V}$, has garnered significant attention throughout the past decade. The

Comparison between Lithium-based and Sodium based energy storage systems is shown in **Table 1**. Nevertheless, challenges persist, particularly concerning inferior electronic conductivity and structural instability at high charging potential. The SICs is an emerging technology that amalgamates the functionalities of capacitors and batteries to offer a versatile solution for energy storage requirements. It comprises two primary components: one high-capacity cathode and another high-power anode, working in tandem to strike a harmonious equilibrium between energy density and power density.

In the domain of hybrid sodium-ion capacitors, the specific capacity is critically determined based on the cathode material selection, which further extends the knowledge of cyclic stability and rate capability.

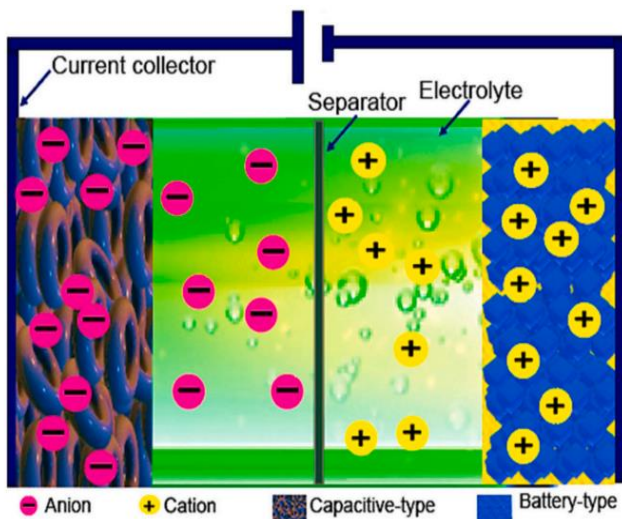


Fig. 4(c). Schematic diagram about charge storage mechanism for Hybrid ion capacitors [8].

Table 1. Comparison between Lithium based and Sodium based energy storage systems

| Lithium based energy storage | Sodium based energy storage |
|---|---------------------------------|
| High energy density | Low energy density |
| Matured technology | Under development |
| Underperformance in extreme temperature | Can work at extreme temperature |
| High initial cost | Low initial cost |
| Material resourcing | Easily available |
| Risk of thermal runaway | Less risk of thermal runaway |
| Scarce in nature | Earth abundant elements |

1.2.3 Fundamental parameters for energy storage in supercapacitors:

The two primary fundamental parameters used to characterize the functioning of energy devices are energy density and power density. power density Indicates how quickly energy can be released, whereas energy density indicates the capacity to store energy. There are two primary energy storage devices: battery, and supercapacitor [7]. Supercapacitors fall as a promising alternative for batteries. It acts like a bridge holding batteries and electrochemical capacitors based on their electrochemical properties.

The Power density (P_d) and energy density (E_d) are depicted with the help of a Ragone plot (**Fig. 3**). This specific plot views the batteries falling in a high-energy profile, whereas Supercapacitors are in the position of a high-power profile. Batteries exhibit power and energy capabilities in an intermediary manner. Also, this plot shows that no electrochemical device could compete with the internal combustion engine. So, the E_d and P_d of the electrochemical devices need to be improved to compete with the combustion engine.

For supercapacitors, the E as well as the P can be calculated by:

$$E = \frac{1}{2} CV^2$$

$$P = \frac{V^2}{4R}$$

Where V is the operating voltage, C represents specific capacitance and R is ESR.

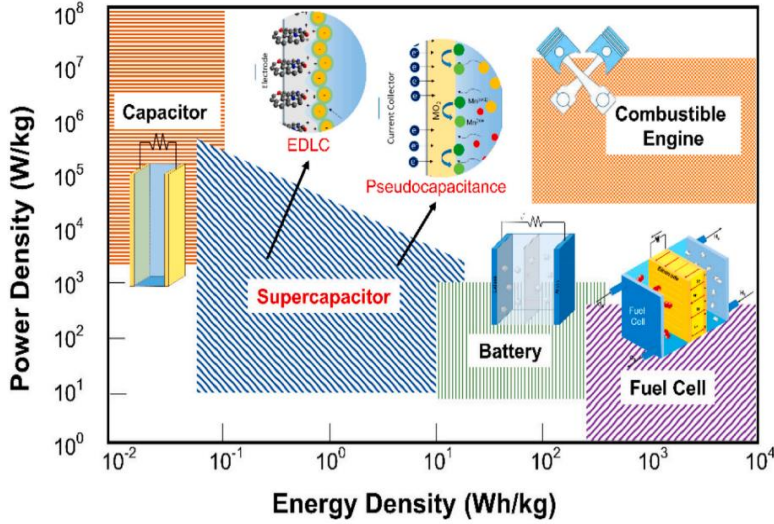


Fig. 5. Ragone plot of energy storage device [7].

1.2.4 Materials for supercapacitors:

Based on the type of capacitance to be used, a variety of materials can be used to create supercapacitors. **Fig. 6** shows the classification of electrode materials for electrochemical supercapacitors. The most common commercial materials for supercapacitors are:

1.2.4.1 Anode active materials:

(a) Transition metal carbides and/or nitrides (MXenes)

The highly conductive carbide and carbonitride layers that makeup MXenes primarily have hydroxyl- and hydrophilic-terminated surfaces. The general formula $M_{n+1}AX_n$ can be used. These are created by etching the "A" layers selectively from their parent MAX phases, where n = 1, 2, or 3. M is the transition metal (Ti, V, Cr, Mn, Zr, Nb, Mo, or Ta), and A is one of a group of 13 or 14 elements (Al, Ga, In, Si, Ge, As, Sn, or Pb), and X can be either or both carbon or nitrogen. The stacked structure of MXenes as well as transition metal M provide MXenes with the ability to

transfer charges and their inherent conductive nature [10]. An increase in capacitance can be achieved through cation exchange (Mg^{2+} , K^+ , Na^+ , Al^{3+} , NH_4^+) which includes variations in charge and size. MXene materials hold great promise for attaining both high energy as well as power densities simultaneously, however making it suitable for a variety of applications on energy storage.

(b) Carbon-based cathode materials:

Materials based on carbon are thought to be promising for use as industrial electrode materials. Carbon-based materials offer many advantages. Their advantages include being widely accessible, reasonably priced, easy to handle, non-toxic, having a significantly greater specific surface area, having satisfactory electrical conductivity, being chemically stable, and having a wide temperature range of operation[11]. High-surface-area carbon materials include carbon aerogels, carbon nanotubes (CNTs), carbon nanofibers, and activated carbon.

1.2.4.2 Cathode active materials:

(a) Metal oxide cathode materials:

Manganese Oxide (M_nO_2) stands as a commonly employed metal oxide cathode material in hybrid sodium-ion capacitors. It boasts a high theoretical capacity and robust cycling stability, making it well-suited for applications requiring a balance between energy and power density. Vanadium pentoxide (V_2O_5) offers high energy density and exceptional electrochemical properties, making it ideal for applications that prioritize energy storage capacity over rapid charge and discharge rates.

(b) Polyanionic cathode materials:

Polyanions are also called sodium superionic conductors such as NASICON have attracted tremendous interest for SICS devices as battery-type electrodes as well as solid electrolytes.

It is mainly due to their extraordinary features, such as high Na^+ ion diffusivity, negligible lattice stress during Na^+ de(insertion), high

ionic conductivity, good chemical & thermal stability, and high operating potential window, rendering the long cyclic life.

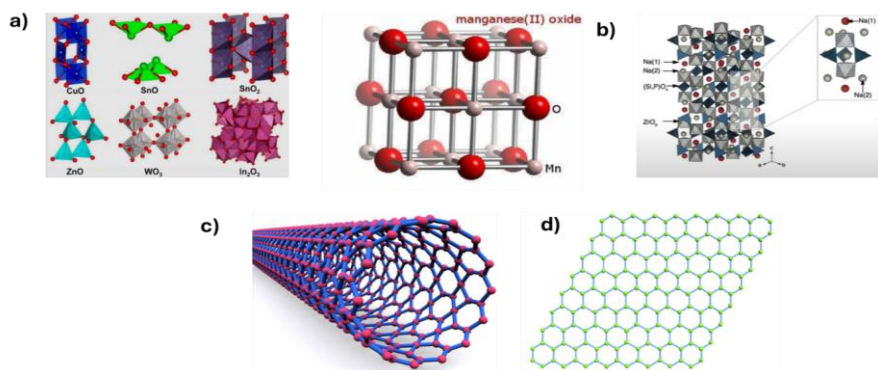


Fig. 6. Classification of electrode materials for electrochemical supercapacitors.

1.2.5 Electrolytes for supercapacitors:

The electrochemical characteristics of supercapacitors are significantly affected by the type of the electrolytes. For supercapacitor cells, P_d can be limited by the resistance of the electrolytes and their specific operating voltage is constrained depending on the breakdown potential of such electrolytes, which limits the energy density. Aqueous and organic electrolytes are the two primary types of electrolytes utilized in supercapacitor technology [12]. The supercapacitor's unit cell voltage is often limited to 1 V by aqueous electrolytes because the thermodynamic

Water has an electrochemical window of 1.23V, whereas organic electrolytes permit a unit cell voltage of more than 2V. Acidic and alkaline electrolytes are the most regularly utilized aqueous electrolytes for supercapacitors because of their unique proton transport mechanism and comparatively high conductivities. In an aqueous electrolyte, the proton has the greatest mobility and can chemisorb to a single oxide ion due to its tiny size. A high concentration of electrolytes is needed to sustain high conductivity in order to decrease the ESR and prevent electrolyte depletion issues during charge. Regarding organic electrolytes, they are typically based on propylene carbonate or acetonitrile as solvents that enable

a supercapacitor to function for up to 2.3V. The salts have a comparatively low solubility in the organic solvents.

Table 2. Comparison between Aqueous and organic electrolytes.

| Type of electrolyte | Advantages | Disadvantages |
|---------------------|--|---|
| Aqueous electrolyte | <ul style="list-style-type: none"> • Low cost • High ionic conductivity • Non-flammability • Safe • Compatibility in air and O₂ | <ul style="list-style-type: none"> • Small voltage window • May accelerates degradation of components • High self-discharge |
| Organic electrolyte | <ul style="list-style-type: none"> • Good wettability • Wide operating temperature • Large voltage window • Low self-discharge • Low degradation of Components. | <ul style="list-style-type: none"> • Complex synthesis • Costly • Usually flammable • Low ionic conductivity • High toxicity |

1.3 Thesis Objective and Scope:

Due to its cost-effectiveness and huge abundance of sodium ions adding to its higher energy density than supercapacitors, aqueous SICs are becoming a very popular research topic and NASICON is a promising electrode material. However, there are certain problems that hinder the use of aqueous energy storage systems such as low electrochemical potential windows and low electronic conductivity of the NASICON electrodes. Therefore, the objective of this research is to fabricate advanced NASICON electrodes for SICs with large electrochemical potential window. In this regard, the objectives are formulated as follows,

- a) Optimization of the electrochemical potential window using high-concentration perchlorate electrolyte in three-electrode cells.
- b) Development and investigation of Ce-modified NVPs ($\text{Na}_3\text{V}_{2-x}\text{Ce}_x(\text{PO}_4)_3$, $x=0.02, 0.04, 0.06, \text{ and } 0.1$).
- c) Investigation of physiochemical and electrochemical characterizations of the as-synthesized electrode materials.
- d) Performance evolution of full cell using $\text{Na}_3\text{V}_{2-x}\text{Ce}_x(\text{PO}_4)_3/\text{MXene}$ device under optimized electrolyte concentration.

1.4 Organization of the Thesis:

The main goals of this dissertation are to create electrode materials that can store energy through redox reactions as well as surface adsorption and investigate novel materials with superior electrochemical performance. The thesis has been organized into three chapters, which are explained in more detail below:

Chapter 1 outlines the need for supercapacitor research as well as the global situation regarding supercapacitors today. It also provides some background information on the development of supercapacitors as well as the characteristics and properties of the materials that will be synthesized so that readers will understand the rationale behind our material selection.

Chapter 2 described the experimental methods used for the scheme and preparation of materials, the electrochemical system's parts, and electrodes. This chapter also explains the characterization methods applied to the study of the produced electrode material.

Chapter 3 outlines the results of the XRD, TGA, FTIR, FESEM, RAMAN, CV and GCD of the materials.

Chapter 2

Experimental Section

2.1 Chemicals

The citric acid ($C_6H_8O_7$), Ammonium metavanadate (NH_4VO_3), Sodium dihydrogen phosphate dehydrated ($NaH_2PO_4 \cdot 2H_2O$), Cerium nitrate hexahydrate ($Ce(NO_3)_3 \cdot 6H_2O$), N-Methyl-2-pyrrolidone (NMP), Activated Carbon, Carbon black, Polyvinylidene fluoride (PVDF), Hydrogen chloride (HCl), Hydrogen fluoride (HF) and Polytetrafluoroethylene were brought from Sigma Aldrich chemicals and Sri Chemicals Pvt. Ltd. and used as it is. Ethanol was also purchased from Sri Chemicals Pvt. Ltd. Deionized (DI) water used all over the experiments was obtained from the Milli-Q system with a resistivity of 18.2 M Ω .

2.2 Synthesis of $Na_3V_2(PO_4)_3$:

NVP was synthesized by the Rheological phase reaction method. The reagents $C_6H_8O_7$, NH_4VO_3 , and $NaH_2PO_4 \cdot 2H_2O$ with stoichiometric ratio of 2:3:2 were added together in an agate mortar to form a homogenous mixture[13]. After this, the homogenous mixture with a few drops of water was shifted into a Teflon-lined container under stirring to create a rheological phase solution. Then, the Teflon-lined autoclave was heated for 8 hrs at 80°C. After 8 hrs, the gel sample was collected from the autoclave and kept for drying under a vacuum oven for 12 hrs at 100°C. The attained powder was placed inside a tubular furnace and heated at 350°C for 3 hrs in an argon atmosphere and annealed for 8 hrs at 800°C with a rate of heating 3°C /min.

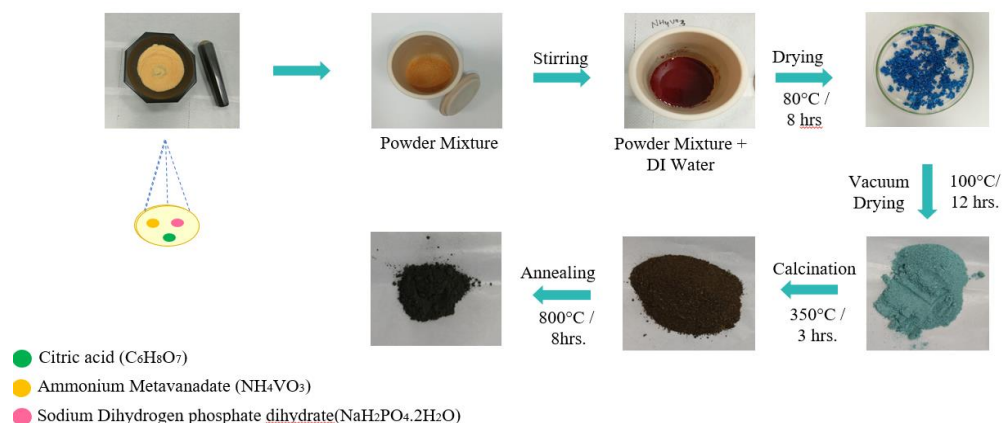


Fig. 7. Schematic diagram of the preparation process of $Na_3V_2(PO_4)_3$

2.3 Synthesis of $Na_3V_{2-x}Ce_x(PO_4)_3$:

$Na_3V_{2-x}Ce_x(PO_4)_3$ was prepared by the Rheological phase reaction method. The reagents $C_6H_8O_7$, $Ce(NO_3)_3 \cdot 6H_2O$, NH_4VO_3 , and $NaH_2PO_4 \cdot 2H_2O$ with the stoichiometric ratio of 2:2-x:x:3 where $x=0, 0.02, 0.04, 0.06, 0.1$ were added together in an agate mortar to form a homogenous mixture [14]. After this, the homogenous mixture with a few drops of DI water was shifted into a Teflon-lined container under stirring to attain a rheological phase solution. Then, the Teflon-lined autoclave was heated for 8 hrs at 80°C. After 8 hrs the gel sample was collected from the autoclave and kept for drying in a vacuum oven for 12 hrs at 100°C. The attained powder was placed inside a tubular furnace and heated at 350°C for 3 hrs in an argon atmosphere and annealed for 8 hrs at 800°C with a rate of heating of 3°C /min.

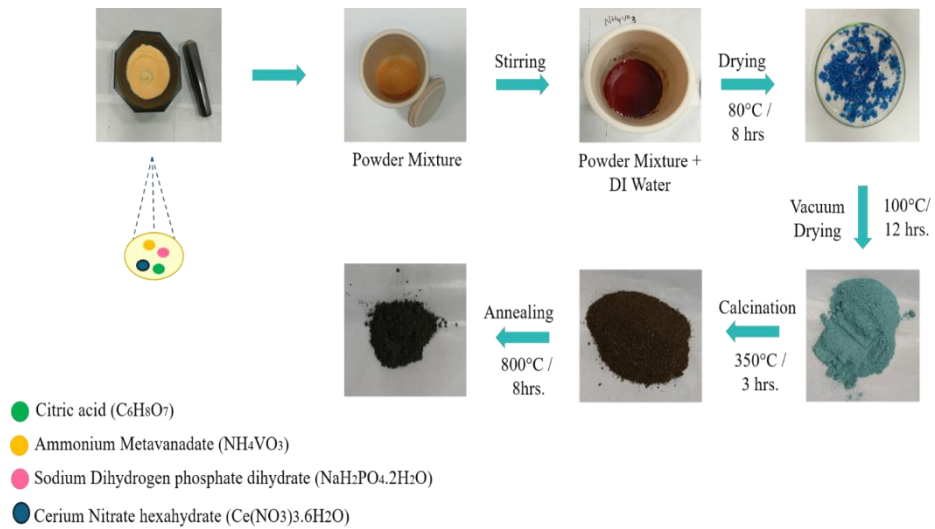


Fig. 8. Schematic diagram of the preparation process of Na₃V_{2-x}Ce_x(PO₄)₃ (x=0, 0.02, 0.04, 0.06, 0.1)

2.4 Synthesis of MXenes:

MXene (Ti₃C₂T_x) was synthesized by using the selective etching method. First 6 mL of DI- water, 12 mL HCl, and 2 mL HF to a Teflon container. After that add slowly 1.0 g MAX Phase into the solution and stir for 5min at 45°C with 350 RPM[10]. The reaction proceeds for 24 hrs. This suspension was later centrifuged at 4000 rpm for 10-15 min by using Ethanol and DI water until the pH of the suspension attained nearly neutral that is less than 6. The material obtained was dried at 60°C for 8 hrs in a vacuum oven.



Fig. 9. Schematic diagram of the synthesis process of MXenes.

2.5 Material characterization

By using P-XRD, the crystallinity, crystal structure, and phase change were confirmed. With a step size of 0.02 and a wavelength of 1.54 Å, the diffraction patterns of the materials were recorded using Cu Kα radiation as the source of X-ray in the 2θ

range of 10-70° on the PANalytical X-ray diffractometer. XPS-Thermo Fisher Scientific ESCALAB was used for investigating X-ray photoelectron spectroscopy (XPS)[15]. Thermogravimetric analysis (TGA) was obtained using a Perkin Elmer device from room temperature to 800°C at a rate of heating of 10°C/min under a nitrogen environment to determine the thermal stability of the material and its segment of volatile components. The Field emission scanning electron microscopy (FESEM) (JEOL-7610F Plus) equipped with energy dispersive spectroscopy (EDS) and transmission electron microscopy (TEM)(FEI-TALOSF200S) was used to visualize very small topographic details on the surface and for morphological and elemental analyses.

To identify the functional organic and inorganic groups Fourier transform infrared spectra (FTIR) of the NVP and Ce-doped NVP are recorded with the help of Perkin Eimear ATR spectrometer over the range of 400 to 4000 cm^{-1} wavenumber. Micro-Raman spectra were obtained from an InVia Raman micro spectrometer (Labram Horiba) with 514.5 nm radiation at a laser power of 0.4 mW in the range of 0–2000 cm^{-1} .

2.6 Modification of the working electrode

2.6.1) Preparation of Cathode material:

To evaluate the electrochemical performance of a Hybrid ion capacitor, the working electrode was modified by as-synthesized material¹⁵. Firstly, stainless steel as a current collector was cut and washed with DI water and ethanol for a certain time and kept for drying properly in an oven at room temperature. After that the slurry of active material in the ratio of (7:2:1) working material: carbon black: PVDF and NMP solution was prepared. Carbon black was used as a conducting material and PVDF was used as a binder. Then 2mg slurry was coated on the current collector such as stainless steel by drop cast method and dried overnight. This synthesized electrode was treated as a working electrode.

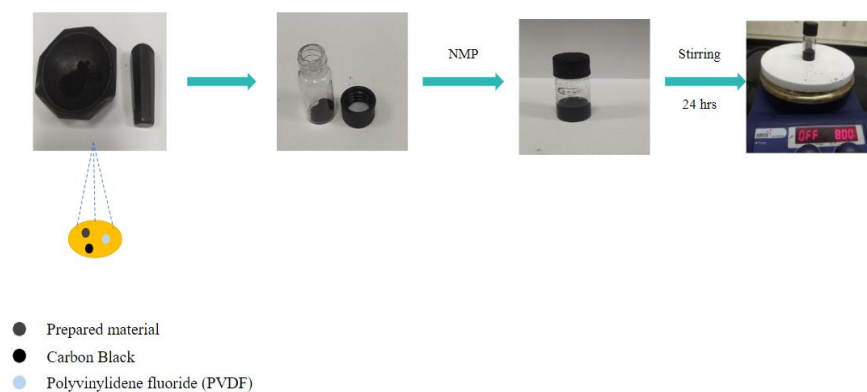


Fig. 10. Schematic diagram of the preparation process of a slurry of cathode material.

2.6.2) Preparation of Anode material:

In three-electrode electrochemical characterization as an anode material, we used activated carbon. This electrode was prepared by using Activated Carbon, Carbon black, and PTFE in (8:1:1) ratio. PTFE was used as a binder. Firstly, by using the mortar and pestle, we mixed the powders and by using PTFE solution made a paste and applied this paste on a current collector as a stainless steel. After drying, apply pressure to compact the electrode. This electrode was used as a counter electrode in three-electrode electrochemical characterization.

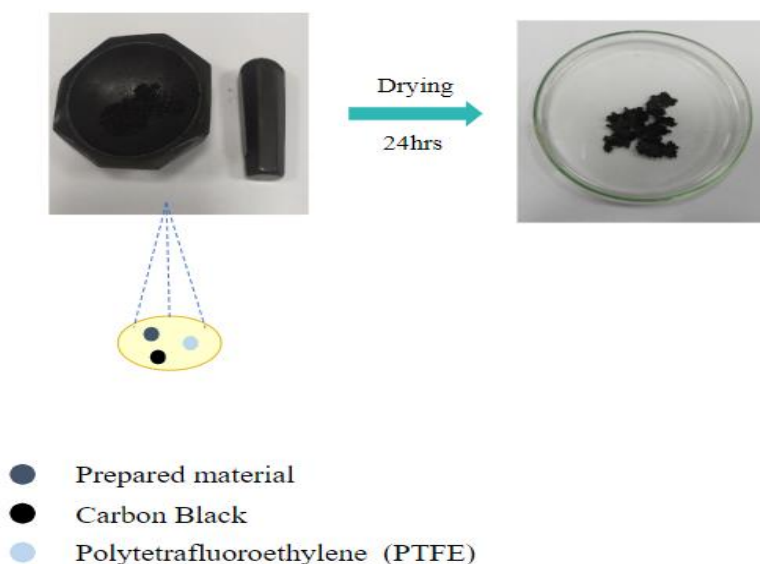


Fig. 11. Schematic diagram of the preparation process of a slurry of anode material.

2.7 Preparation of electrolyte:

To prepare WIS electrolytes, ionic substances such as sodium perchlorate monohydrate are dissolved in a solvent such as DI water to the appropriate molarity. Initially, the volume of solution in L, molarity in M, and Molar mass of the sodium perchlorate were specified. A 5 ml vial was taken and 1 ml of deionized water was added. Gently, 2.3g of sodium perchlorate monohydrate was added to the vial preparing a 1M concentrated solution followed by continuous stirring to ensure it dissolved completely.



Fig. 12. Schematic diagram of the preparation process of electrolyte.

2.8 Electrochemical measurements:

For electrochemical analysis, Autolab 204 potentiostat with a standardized three-electrode Swagelok cell setup one termed as working electrode which is active material, the counter electrode is Activated Carbon, and the reference electrode is Ag/AgCl in different concentrations of sodium perchlorate NaClO₄ [16]. **Fig. 13** shows the Fabrication of three-electrode Swagelok cell. The electrochemical measurements which include CV, GCD, and EIS were performed with a 17m NaClO₄ electrolyte. Because aqueous electrolytes have exceptional thermal and chemical stability, affordability, and high conductivity, it has a limited stability voltage of 1.23V. By using a WIS electrolyte, the stability window of the SICs may be expanded to 2–3.2 V. These outcomes were caused by the minor number of freely water molecules, which suppress the evolution processes of hydrogen and oxygen. Hence, the highly

concentrated electrolyte medium can appear to be one of the techniques to boost aqueous sodium-ion capacitors.

A potential ramp is applied to the working electrode in a CV scan by raising the potential to a limit and then reversing the scan back to the starting potential. The graph that is produced is known as a voltammogram. The specific capacitance was calculated by dividing the integrated area of the voltammogram by the product of the voltage window (V) and scan rate, which is expressed in Farads. The rate at which the scan is applied determines the scan rate. CV studies were performed within a potential range of -1.2 to 1.5V versus Ag/AgCl at scan rates of 1-10 mV /s.

The GCD profile is used to measure the potential versus time response while controlling the current density. This charge-discharge curve can be used to extract important characteristics such as capacity, energy density, power density, and cyclic stability. GCD was done under the potential window of -1.2 to 1.5V at the different current densities of 0.5-5 A/g. EIS was done in the frequency of 10 mHz and 100 mHz in 10 mV AC amplitude.

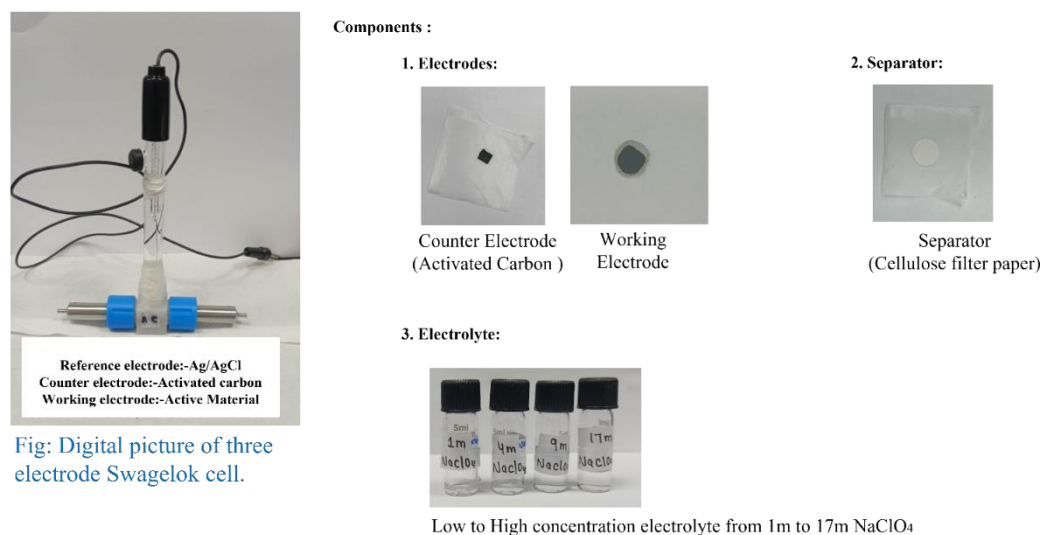


Fig: Digital picture of three electrode Swagelok cell.

Fig. 13. Fabrication of three-electrode Swagelok cell.

2.9 Device fabrication:

Using coin cells with a 16 mm diameter, the SICS was fabricated. Initially, the slurry of the cathode materials such as NVP and Ce-doped NVP were prepared by blending 70% active

materials, 20% Carbon black, and 10% PVDF in NMP solution and the slurry of anode material MXenes for fabricating device was prepared by blending 80% active materials, 10% Carbon black, and 10% PVDF in NMP solution. The resulting slurry was spread over a stainless steel current collector and dried overnight in an oven at room temperature. The optimum mass of cathode: anode coated over each electrode was ~ 1: 2.79 mg. Finally, using a cellulose-based separator the prepared electrode materials were sandwiched to make the device fabricated by adding 80 μ l of 17m NaClO₄ electrolyte.

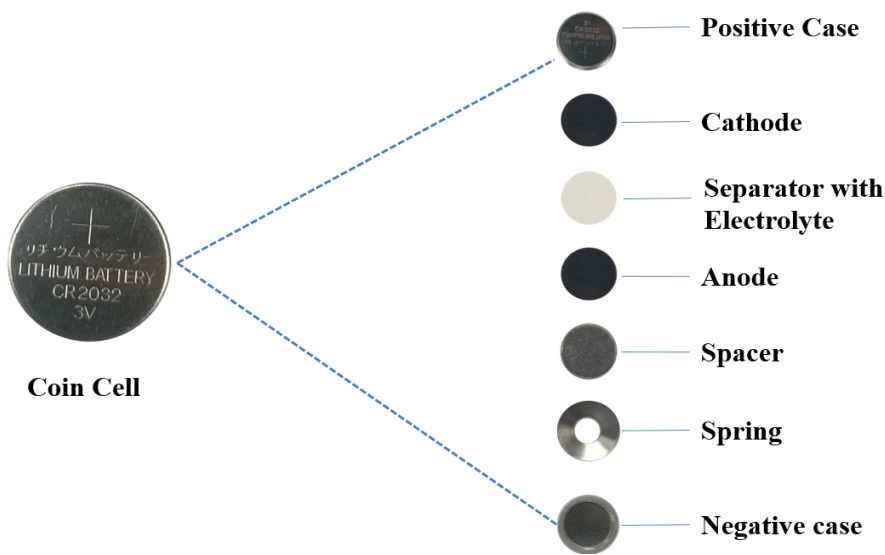


Fig. 14. Fabrication of coin cell.

2.10 Performance Indicators:

Mass balancing equation:

$$\frac{M_a \times C_c}{M_c \times C_a}$$

Where M_a is the active mass of the anode, M_c depicts the active mass of the cathode in mg, C_c represents the specific capacity of the cathode and C_a is the specific capacity of the anode material in mAhg^{-1} .

Specific capacitance and Specific capacity:

$$C = \frac{I\Delta t}{m\Delta V}$$

$$Cp = \frac{I\Delta t}{3.6 \times m}$$

Where C represents the specific capacitance in F/g, Cp is the specific capacity in mAhg⁻¹, I is the current in A, Δt is the discharge time in s, m is the mass coated on the electrode in g and ΔV is the applied voltage range.

The energy density and Power density of the fabricated device were estimated from the GCD curves using the following equations.

$$E_d(\text{Wh/kg}) = \frac{C\Delta V^2}{(2 \times 3.6)}$$
$$P_d (\text{W/kg}) = \frac{3600 \times E_d}{\Delta t}$$

Where E_d is the energy density (Wh/kg) and P_d(W/kg).

Chapter 3

Result and Discussion

3.1 Physical characterization:

3.1.1 X-ray diffraction pattern of materials:

Powder X-ray diffraction (P-XRD) patterns were used to determine the crystal structures and phase purity of all the components, and it is also used to get information about the formation of crystal structures. P-XRD of $\text{Na}_3\text{V}_{2-x}\text{Ce}_x(\text{PO}_4)_3$ is shown in **Fig 15(a)**. The peaks of materials at 2θ : 14.3° , 20.11° , 22.42° , 23.84° , 24.47° , 28.80° , 31.66° , 32.06° and 35.71° correspond to its (012), (104), (110), (113), (006), (024), (211), (116) and (300) planes, respectively, which confirmed rhombohedral crystal structure with the space group of R3c (JCPDS file no. 62-0345)[14]. This fig also reveals that the amount of Ce-doping in the pure material doesn't have any effect on the original rhombohedral crystal structure.

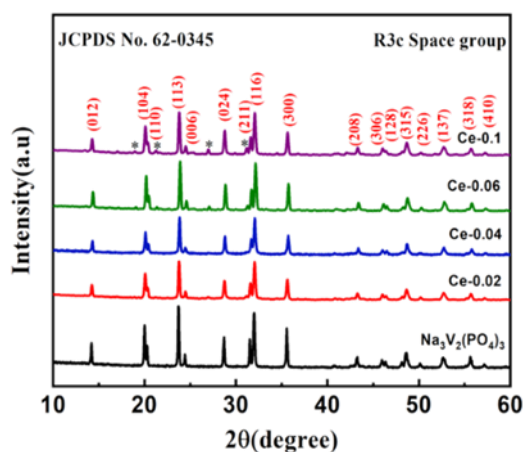


Fig 15. XRD patterns of Ce- doped NVP

3.1.2 XPS spectra:

The elemental confirmation and respective oxidation states of Ce- doped NVP ($x = 0, 0.02, 0.04, 0.06, \text{ and } 0.1$) were examined by analysing XPS as depicted in **Fig.16**. The existence of multiple elements in Ce-doped NVP measured by comprehensive spectra

shown in **Fig.16(a)**. **Fig.16(b)** depicted that the binding energy of Na 1s is 1071.62 eV. **Fig. 16(c)** shows $2p_{3/2}$ and $2p_{1/2}$ core levels of V with the binding energies at 517.21 and 524.08 eV respectively corresponding to +3 oxidation state, and the characteristic peaks for [17] Ce $3d_{3/2}$ and $3d_{5/2}$ at 904.3 eV, 901.68 eV and 885.63 eV, 881.9 eV respectively, confirm the existence of Ce in its +3 and +4 oxidation state and the satellite peaks for Ce^{+4} at 889.89 eV, 907.4 eV shown in **Fig 16(d)**. It shows that Ce^{3+} and Ce^{+4} coexist in the sample, and they exhibit excellent electrical conductivity. The binding energy of P 2p is 133.4 eV in **Fig. 16(e)**. The O 1s spectrum with peaks at 531.09 eV, 532.62 eV, 531.95 eV and 535.92 eV correspond to V-O, Ce-O, C=O and C-O shown in **Fig. 16(f)**. In the case of carbon (**Fig. 16(g)**), peaks at 284.9, 286.21, and 288.23 eV are attributed to C 1s from C-C/C=C, C=O, C-O, and functional groups respectively. Overall, all the elements with appropriate chemical shifts suggest the successful formation of $Na_3V_{2-x}Ce_x(PO_4)_3$ material.

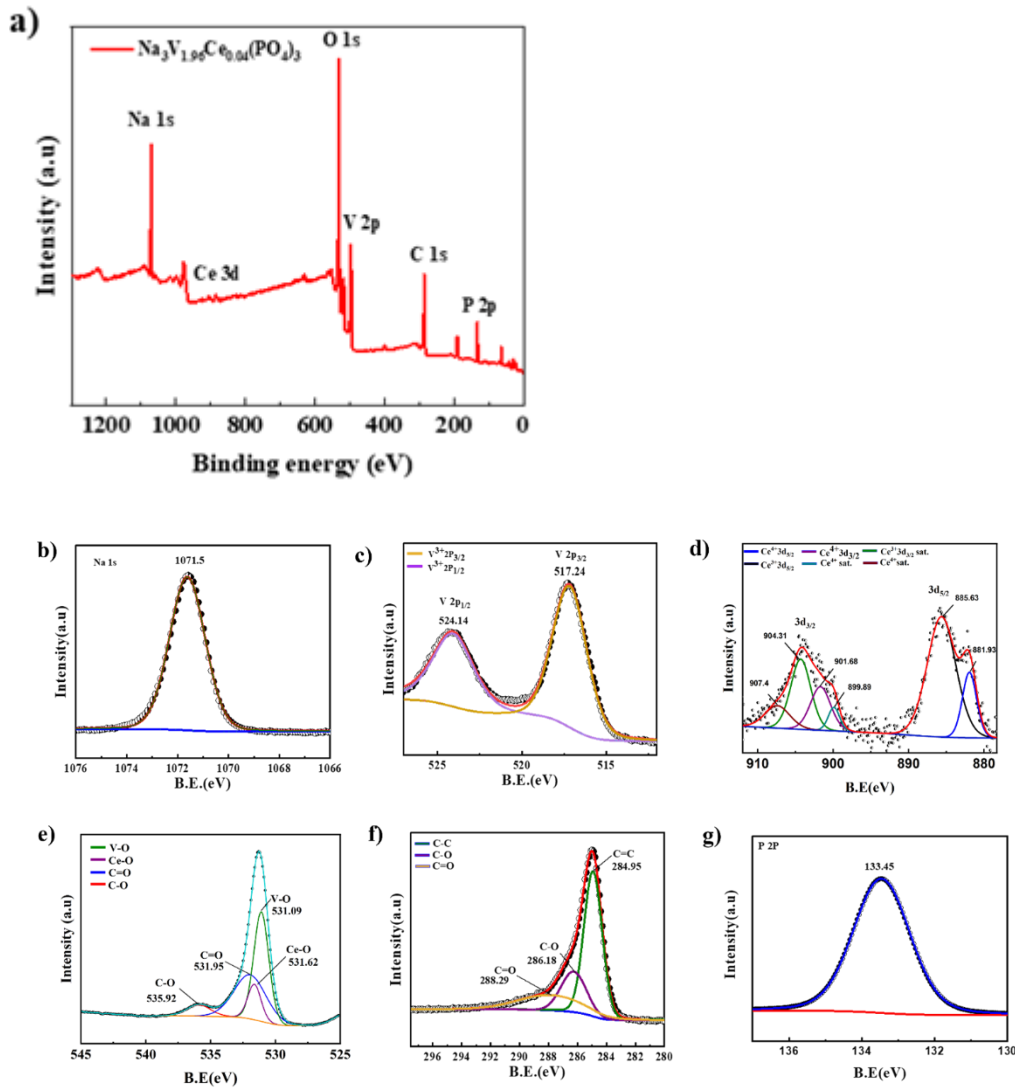


Fig 16. XPS patterns of Ce- doped NVP.

3.1.3 FT-IR spectra

The existence of functional groups is depicted in FTIR spectroscopy. **Fig 17** shows the FTIR result of $\text{Na}_3\text{V}_{2-x}\text{Ce}_x(\text{PO}_4)_3$ from 2000 cm^{-1} to 500 cm^{-1} and the peaks that are visible from this range may provide information on the samples' fine crystal structure. P-O bonds from PO_4 tetrahedra were found at 1021 cm^{-1} , while the vibration from to $\text{V}^{3+}\text{-O}^{2-}$ bonds in VO_6 octahedra was visible at 629 cm^{-1} for all samples[14]. Most of the $\text{Na}_3\text{V}_{2-x}\text{Ce}_x(\text{PO}_4)_3$ compounds have spectra that are in good agreement with the published data.

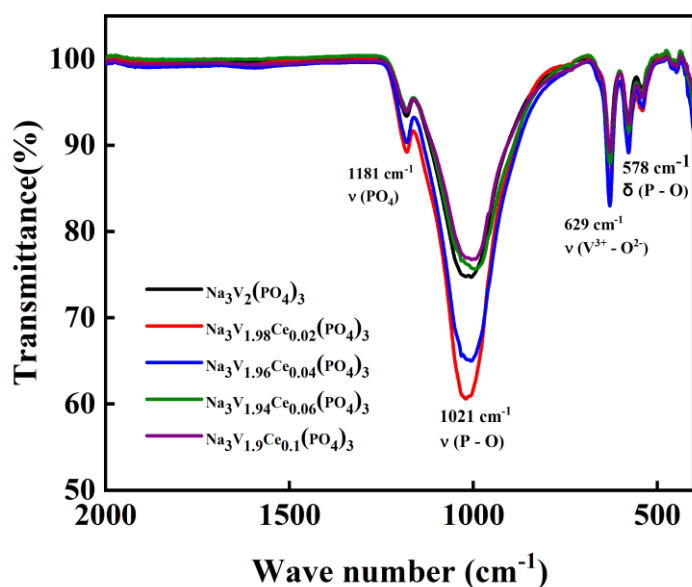


Fig 17. FTIR spectra of Ce- doped NVP.

3.1.4 Morphological Studies:

3.1.4.1: SEM image of materials:

The morphology of Ce- doped NVP material is depicted in **Fig. 18**. From **Fig. 18 (a)**, it can be seen that without Ce ion doped in the material comprised irregular shapes with the inhomogeneous size of the particle [9], and during the calcination process at high temperatures (700°C), the particles are found severely agglomerated, which is adversative to the sodium ion insertion/extraction and the electron transfer during the charging-discharging process. With Ce doping the material showed an extensive uniform morphology and the particle size is different with different concentrations of Ce, it is smaller than pure NVP material when Ce doping is less. While the Ce doping, the crystal growth also increased [18]. It confirmed that with increase in the concentration of Ce had little influence on particle size in Ce-NVP samples shown in **Fig. (18(b-e))**. To identify the content of Ce in prepared samples, Ce-NVP was characterized by EDS, and the results are shown in **Fig. 19 (a-e)**. From the spectra, we clearly

observed the presence of elements of Na, V, Ce, P, O, and C in the doped NVP.

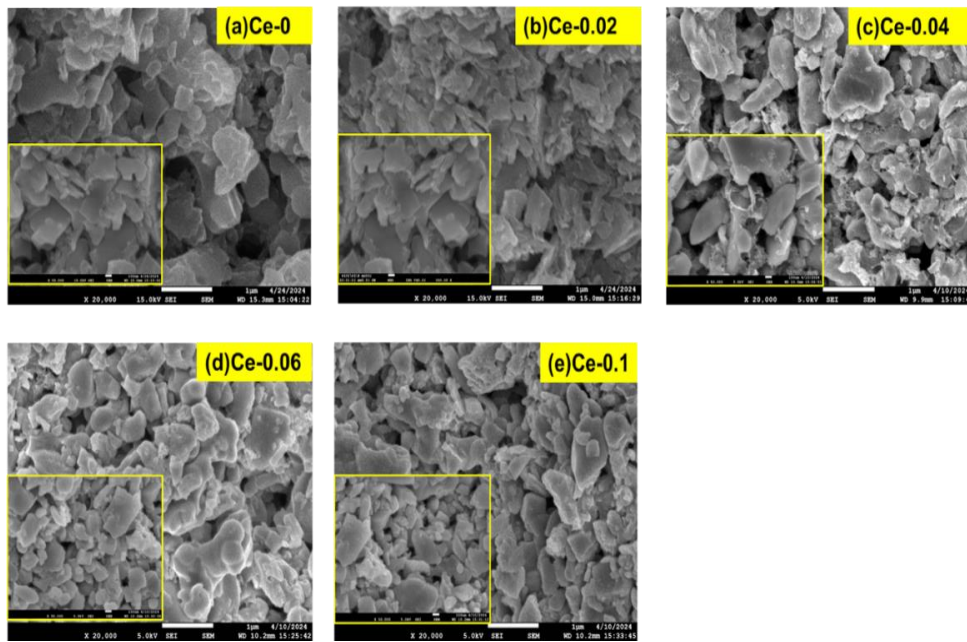


Fig18. FESEM image of Ce- doped NVP samples with different Ce contents: (a) $x = 0$, (b) $x = 0.02$, (c) $x = 0.04$, (d) $x = 0.06$ and (e) $x = 0.1$.

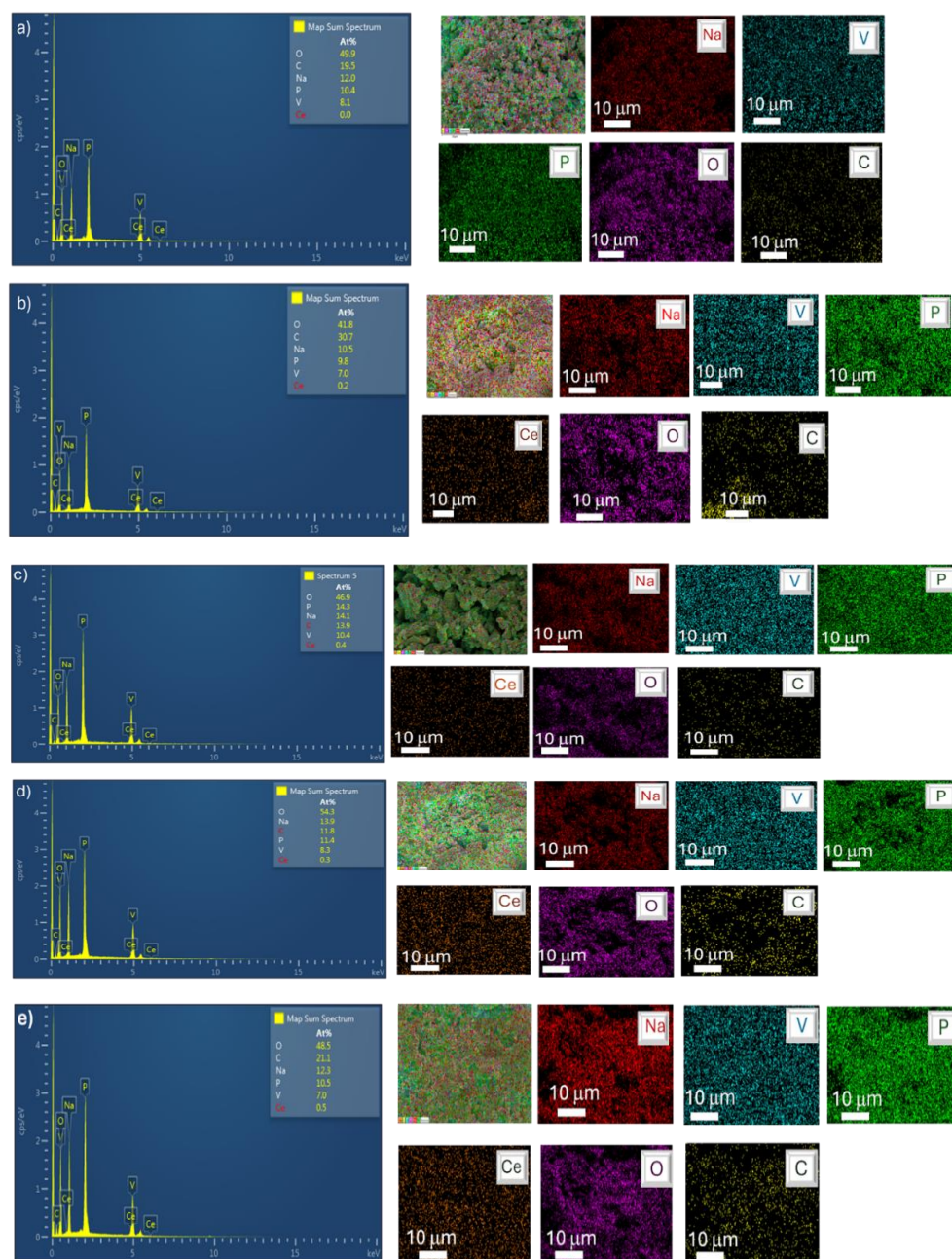


Fig 19. EDX spectra and Elemental mapping of Ce- doped NVP samples with different Ce contents: (a) $x = 0$, (b) $x = 0.02$, (c) $x = 0.04$, (d) $x = 0.06$ and (e) $x = 0.1$.

3.1.4.2: TEM image of materials:

Detailed TEM and HRTEM observations of the sample $\text{Na}_3\text{V}_{1.96}\text{Ce}_{0.04}(\text{PO}_4)_3$ shown in **Fig.20**. **Fig.20(a-b)** shows the TEM image of $\text{Na}_3\text{V}_{1.96}\text{Ce}_{0.04}(\text{PO}_4)_3$, material at different magnifications. The above images confirm the presence of Ce particles stuck to the

Ce-doped NVP material's surface, forming a uniform layer of carbon on the surface of Ce-4 NVP. At the outermost layers of the Ce-4 NVP material more ordered carbon layers can be observed. Additionally, the Ce doping modifies the carbon coating without breaking through the NVP crystals, which are stable chemically and remain on the surface during the heat treatment process[17]. Additionally, a lattice with a (104) crystal plane corresponding to the NVP system and with a spacing of 4.3 Å can be noticed by the HRTEM image in the enlarged image **Fig.20(c-d)**.

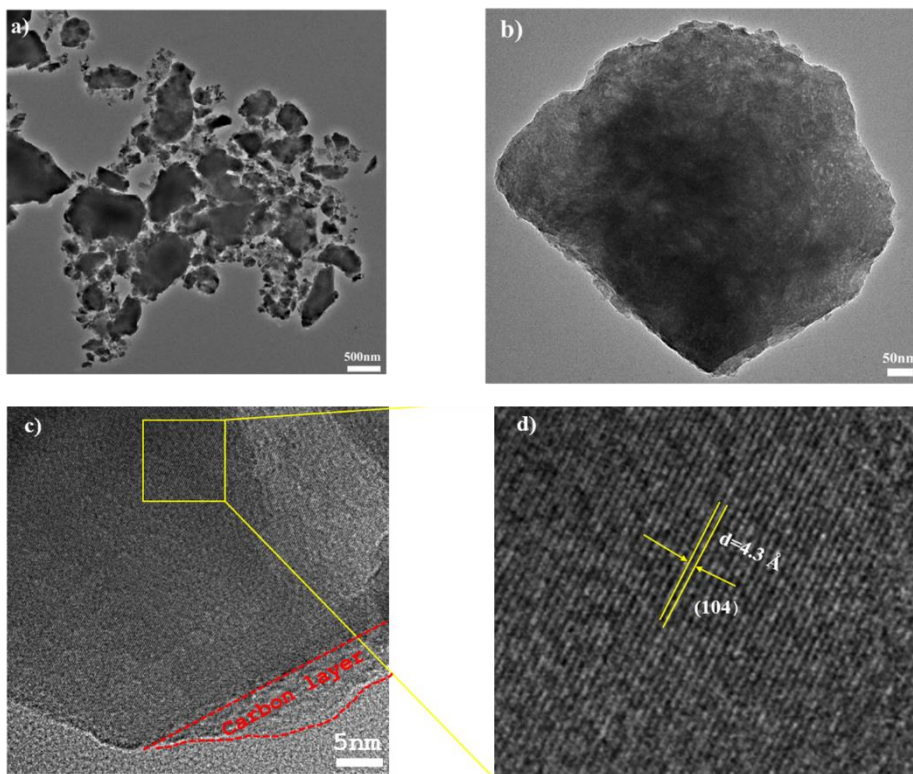


Fig 20. TEM and HRTEM of Na₃V_{1.96}Ce_{0.04}(PO₄)₃.

3.2 Electrochemical performance:

The electrochemical performance of a material is necessary to understand its supercapacitor behaviour. Numerous electrochemical techniques, including GCD, CV, LSV, and EIS, are used to study the electrochemical properties. Since the ESW of aqueous electrolytes directly affects the energy density of electrochemical energy storage devices, research showed interest in

ways to expand the working potential window through varying concentration levels of the electrolyte. NaClO₄ salt was selected for this investigation due to its favourable pricing and excellent water solubility [16]. Extremely high salt-to-water molar ratios in water in salt WIS electrolytes allow for significantly less water activity, which widens the ESW by aggregating highly concentrated cations and anions into a percolating network structure[19]. The anions (ClO₄⁻) and cations (Na⁺) in salt in water (SIW) electrolytes are separated from one another and encircled by a lot of water molecules. Three-electrode Swagelok cells are used to perform one-by-one tests utilizing LSV, CV, and GCD to determine the ESW for salt in water SIW to WIS electrolytes.

3.2.1 Solvent modification for Dissolution Overcome:

ESW of 1m, 4m, 9m, and 17m NaClO₄ electrolytes, was determined by LSV (**Fig 21(a)**). For 1 m NaClO₄, the potential ranged from hydrogen evolution reaction (HER) -1.2 V versus Ag/AgCl to the oxygen evolution reaction (OER) 1.52 V versus Ag/AgCl, achieving 2.72V ESW. Whereas for the 17 m NaClO₄, the potential ranged from HER -1.4 V versus Ag/AgCl to the OER 1.69 V versus Ag/AgCl, achieving an expanded ESW to 3.08V. This ESW is well beyond the thermodynamic potential window of water (1.23V) shown in **Table 3**.

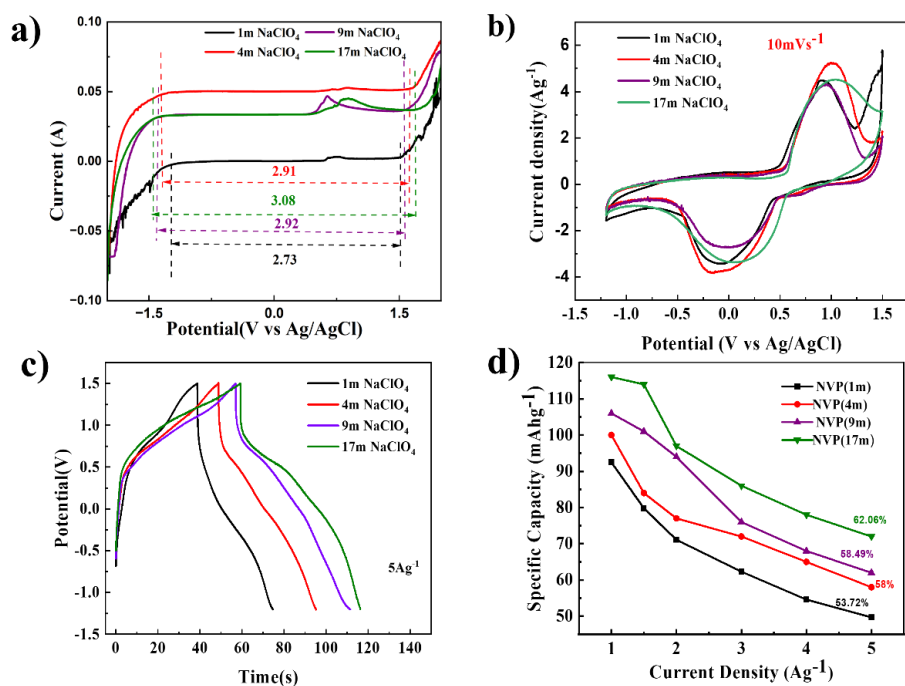


Fig. 21 (a) LSV curve of NVP for low to high-concentration electrolytes, (b) CV profiles of the NVP at 10mVs^{-1} different concentrations of electrolyte; (c) GCD plots of the NVP at 5Ag^{-1} current density with different concentrations of electrolyte, (d) comparison of the change in specific capacity of NVP with different concentration of electrolyte.

Table 3. Variation in the potential window of NVP material with different concentrations of electrolytes: (a) $x = 1\text{m}$, (b) $x = 4\text{m}$, (c) $x = 9\text{m}$, and (d) $x = 17\text{m}$.

| Concentration (m) | Potential (V) | Potential Window (V) |
|-------------------|-----------------|----------------------|
| 1m | -1.22V to 1.5V | 2.73V |
| 4m | -1.35V to 1.56V | 2.91V |
| 9m | -1.35V to 1.54V | 2.92V |
| 17m | -1.4V to 1.68V | 3.08V |

CV curve of NVP at (10-50 mVs^{-1}) scan rates with 1 m, 4m, 9m, and 17m NaClO_4 , is shown in **(Fig. 21(b))**. During charging the sodium ions de-intercalate from the cathode material NVP and migrate within the electrolyte towards the anode. Simultaneously, anions in the electrolyte migrate towards the cathode to maintain charge neutrality [20]. At the anode, sodium ions intercalate into or adsorb onto the anode material. From the CV curve, it is seen that the area of the curve for 17m NaClO_4 (94×10^{-4}) is greater than the area of 1m NaClO_4 (91×10^{-4}) at 10mVs which depicts that at high concentration electrolyte, it provides a wider potential window followed by confirming through GCD plot, according to GCD plot of NVP in 17m NaClO_4 gives more value of specific capacity (57.09 mAhg^{-1}) compared to the specific capacity(35.81 mAhg^{-1}) in 1m NaClO_4 at 5 Ag^{-1} current density, as shown in **(Fig. 21(c))** and also improving rate capability from 53.72 % to 62.06 % **(Fig. 21(d))**. **Fig. 22** shows the CV curve for NVP material in low to high-concentration electrolytes performing at different-different scan rates from 10 to 50 mV s^{-1} and **Fig.23** shows the GCD curve at different-different current densities(0.5 Ag^{-1} to 5 Ag^{-1}).

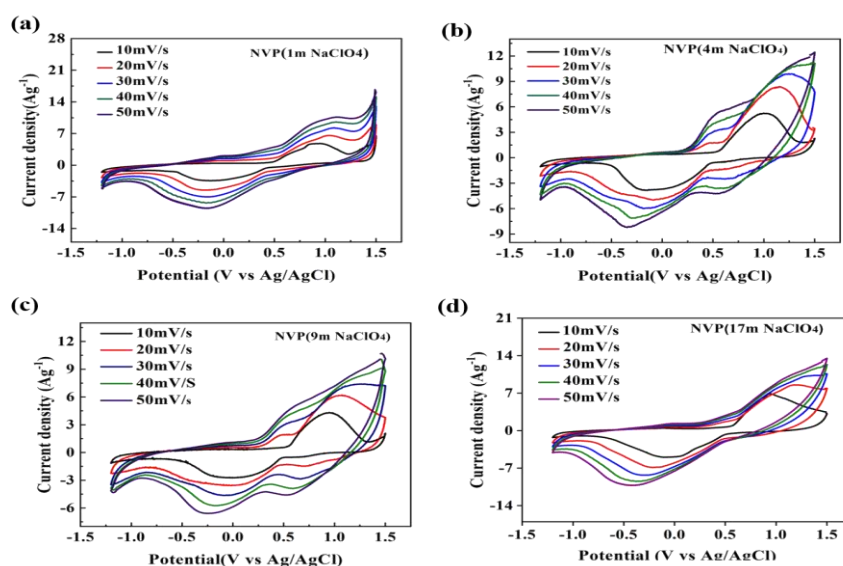


Fig. 22 CV profiles of NVP at (10-50 mVs^{-1}) scan rates with different concentrations of electrolytes: (a) x = 1m, (b) x = 4m, (c) x = 9m, and (d) x = 17m.

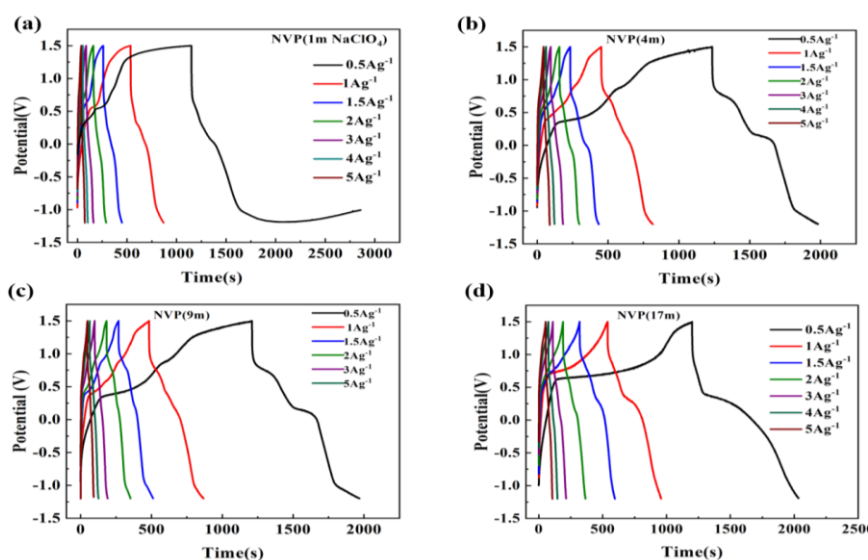


Fig. 23 GCD plots of the NVP at ($0.5 - 5 \text{ Ag}^{-1}$) current density with different concentrations of electrolytes: (a) $x = 1\text{m}$, (b) $x = 4\text{m}$, (c) $x = 9\text{m}$, and (d) $x = 17\text{m}$.

From the initial optimization, the 17m NaClO_4 “water-in-salt” electrolyte was selected as it is owing towards the best performance for the NVP electrode compared to the 1m NaClO_4 electrolyte. We found that the separators in the 1m NaClO_4 electrolyte medium turned yellow after certain cycles, hence implying the dissolution of V elements; moreover, there was not any significant change in colour for the 17m NaClO_4 (**Fig. 24**)(a).Cyclic performance of NVP with 1m and 17m concentrations of NaClO_4 Electrolyte at 5Ag^{-1} current density shown in (**Fig. 24**)(b) which also shows that the 17m NaClO_4 exhibit good cyclic ability as compared to 1m NaClO_4 . Current research reveals that aqueous electrolytes with high concentration tend to have a distinctive hydration cluster with few free water molecules, [21]providing an extended electrochemical stability window and mitigating the material dissolution issue and thus improving cyclic stability.

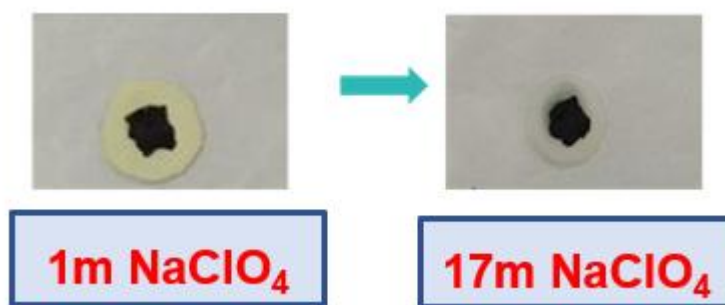


Fig. 24 (a) Digital picture of Separator after cycling.

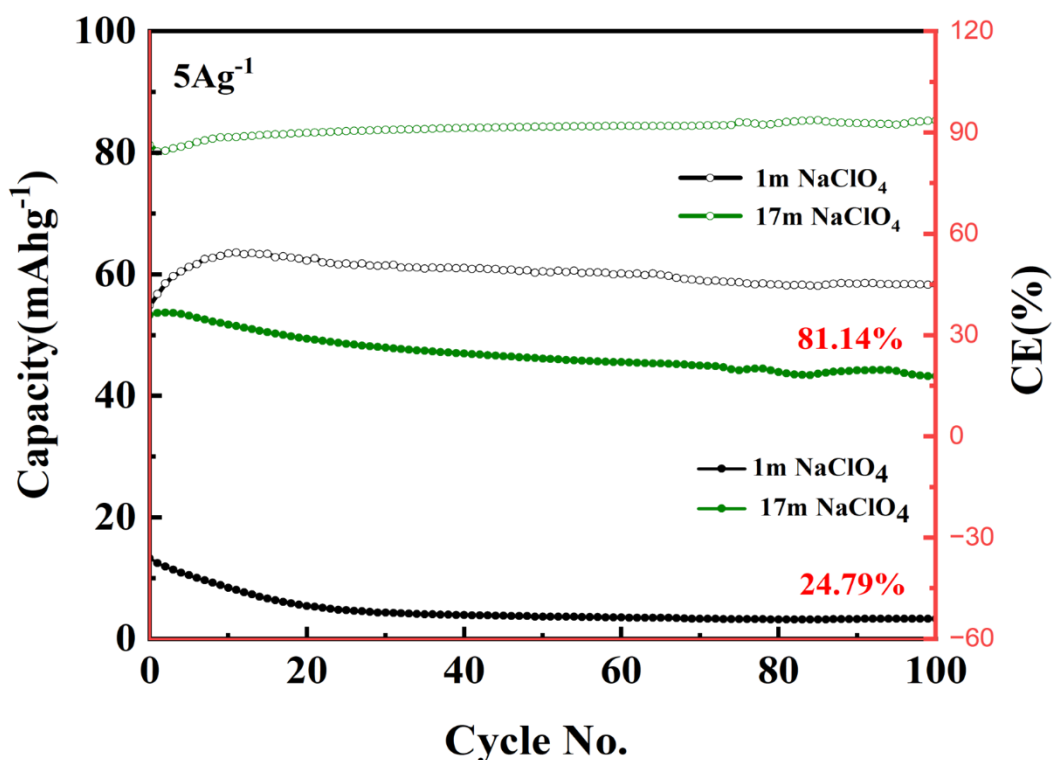


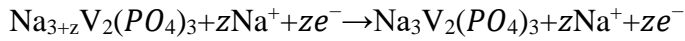
Fig 24(b) Cyclic performance of NVP with 1m and 17m concentrations of NaClO₄ electrolyte at 5A/g current density.

3.2.2 Three electrode Characterization:

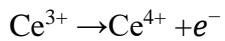
Fig.25 shows the three-electrode electrochemical performance in 17 m NaClO₄ of Ce- doped NVP which was used as a cathode material for the sodium ion hybrid capacitors (SICs) in this work. The CV plot of the Ce- doped NVP electrode at 10mVs⁻¹ shown in Fig.25(a) which depicts two pairs of redox peaks at 0.69/0.08V and 1.12/0.61 V (vs. Ag/AgCl), which confirmed the Na⁺ intercalation/deintercalation from the NVP structure. In the fully charged state, Na₃V₂(PO₄)₃ has all its vanadium atoms in the V³⁺

state. During charging, Na^+ ions are isolated from the structure, and the vanadium is oxidized from V^{3+} to V^{4+} . During discharging, sodium Na^+ ions intercalate into the NVP structure from the electrolyte, and the vanadium is reduced from V^{4+} to V^{3+} . Ce doping in NVP can introduce additional redox reactions because of its redox-active ability to switch among Ce^{3+} and Ce^{4+} .

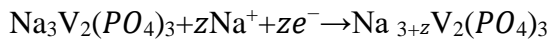
During deintercalation (Charging):



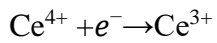
And Ce is involved



During intercalation (Discharging):



And Ce is involved



Here, z represents the number of sodium ions intercalated/deintercalated.

Fig.25 (b) shows the charge-discharge curves of as-prepared Ce-doped NVP materials at 5Ag^{-1} using the voltage range of -1.2 to 1.5 V for the second cycle. The specific discharge capacities were 72, 76.8, 79.16, 73.48, and 63 mAhg^{-1} at the current density of 5Ag^{-1} .

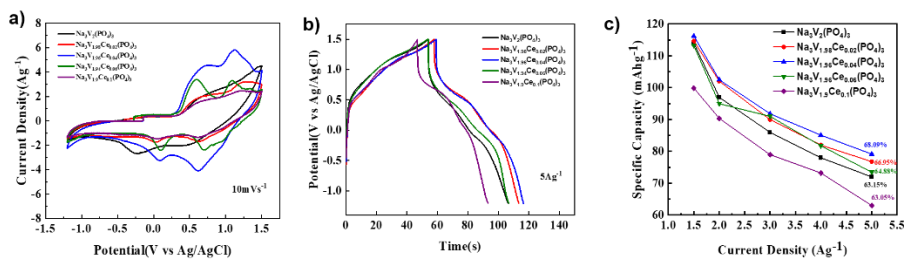


Fig. 25 (a) CV profiles of the Ce- doped NVP at 10mVs^{-1} ; (b) GCD plots of the Ce- doped NVP at 5Ag^{-1} , (c) comparison of the change in specific capacity of Ce- doped NVP at different current density. The comparison between the GCD profile of Ce-0 NVP and the Ce-4 NVP shows that Ce-4 NVP is giving higher discharge time as compared to Ce-0 NVP and then the specific capacities is also higher in case of Ce-4 NVP ¹⁴Smaller polarizations view in the discharge curve profile of the Ce- doped NVP ($x = 0.02, 0.04,$ and

0.06) electrode is the consequence of quick extraction/insertion of sodium ions and its electron transfer, which is made probable due to the reduced size of the particle and enhanced homogeneity with a moderate quantity of Ce doping.

Nevertheless, if the doping concentration is higher than the ideal level, the extra Ce will cause the particle size to increase and will produce inactive impurities, which will lower the initial specific capacity. Therefore, for the Ce- doped NVP samples with $x = 0, 0.02, 0.04,$ and 0.06 , the discharge specific capacity exhibits an increasing first and then decreasing trend with an increase in Ce doping and rate capability also improved from 63.15 % to 68.09 % shown in **Fig.25(c)**. **Fig.26** shows the CV curve of Ce-doped NVP materials at different scan rates and **Fig.27** shows charge-discharge profiles of Ce- doped NVP ($x = 0, 0.02, 0.04, 0.06,$ and 0.1) at various current densities.

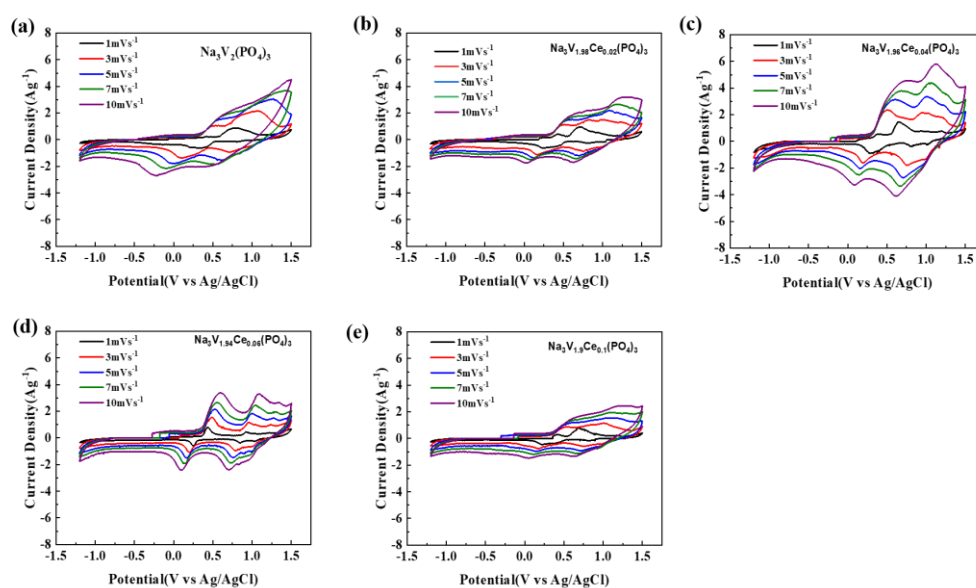


Fig. 26 CV profiles of theCe- doped NVP samples with different Ce contents: (a) $x = 0$, (b) $x = 0.02$, (c) $x = 0.04$, (d) $x = 0.06$ and (e) $x = 0.1$ at different scan rate.

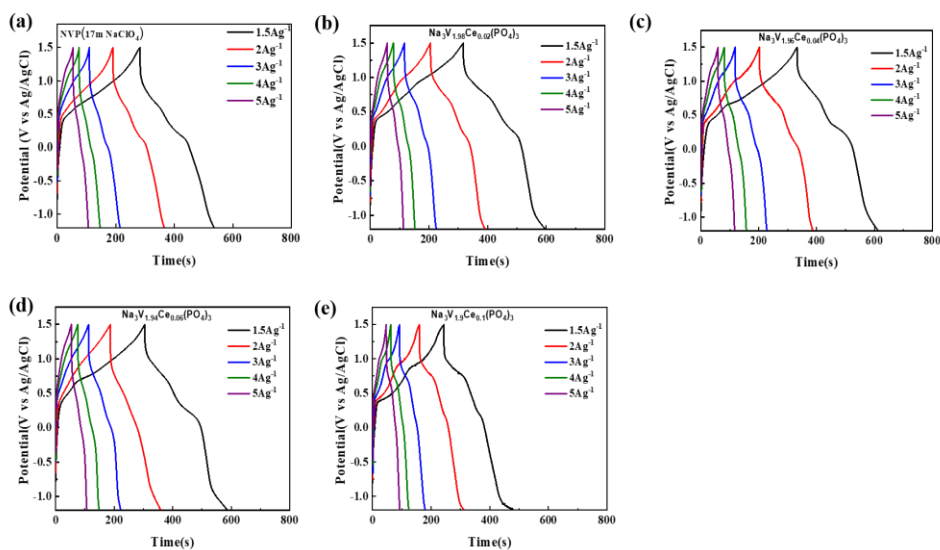


Fig. 27 GCD plots for the Ce- doped NVP samples with different Ce contents: (a) $x = 0$, (b) $x = 0.02$, (c) $x = 0.04$, (d) $x = 0.06$ and (e) $x = 0.1$ at different current density.

To understand the charge storage mechanism, ion transportation, conductive nature, and charge transfer kinetics EIS is carried out. Nyquist plots for the Ce- doped NVP are shown in **Fig.28** with an AC amplitude of 10 mV in the frequency range of 10 mHz to 100 kHz in 17m NaClO₄ electrolyte solution.

The intercept of the impedance line with the real axis in the Nyquist plot gives the equivalent series resistance (R_s) of electrolyte resistance and contact resistance at the electrode and electrolyte interface. Nyquist plot of the Ce- doped NVP samples with different Ce contents shown in **Fig.28(b)**.

Bode plot for the Ce- doped NVP is shown in **Fig.28(a)** which shows the impedance phase angle variation with frequency at an amplitude of 10 mV of AC voltage. This plot also renders information about the capacitive nature of the material. Impedance phase angle at low frequency indicates the ideal capacitive nature of the material.

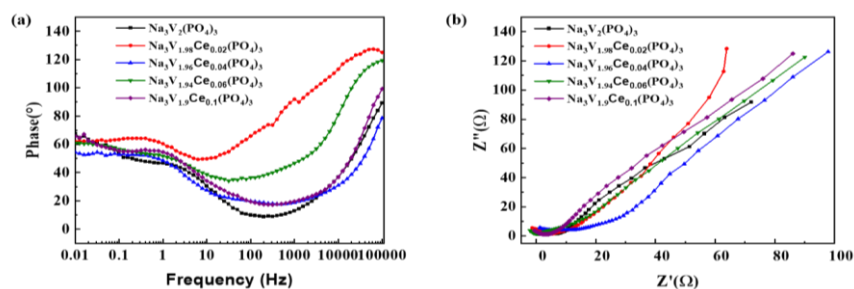


Fig. 28 EIS spectra of the Ce- doped NVP samples with different Ce contents: (a) Bode plot,(b) Nyquist plots.

3.2.3 Two Electrode Characterization:

Electrochemical performances of the Ce- doped NVP cathode were evaluated in coin-type full-cells with MXenes anodes in 17 m NaClO₄ electrolyte for the ASICSSs. Based on the specific capacity of NVP cathodes and MXene anodes from a three-electrode system, the cathode/anode mass ratio was adjusted to 1:2.79 for compensating the irreversible Na loss performed during the preceding cycle. The CV curves of the Ce- doped NVP electrodes at 10mVs⁻¹ scan rate were shown in **Fig 29(a)** it is seen that area of CV curve for Ce-4 NVP is greater than the area of the curve in NVP. GCD curves the Ce- doped NVP samples at 1Ag⁻¹ current densities with the potential window range of 0.01V – 2.2 V shown in **Fig.29 (b)** which shows the specific capacities 41.94, 63.87,65.86,57.93, and 45.46 mAhg⁻¹ for the Ce- doped NVP samples. Rate performance also improved from 33.07% to 38.78 % shown in **Fig.29(c)**.

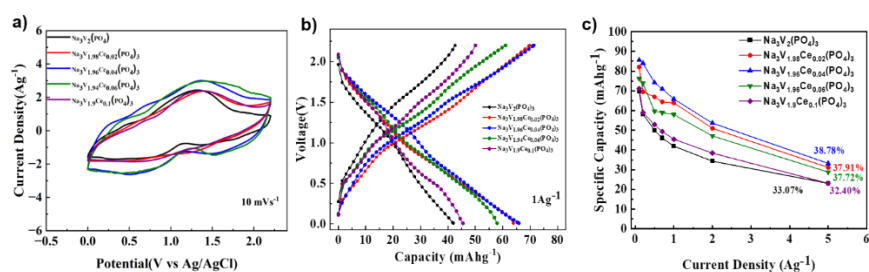


Fig. 29 Electrochemical performances of the Ce- doped NVP in two electrode. (a) CV profiles of Ce - NVP at 10mVs⁻¹; (b) GCD plots of Ce - NVP at 1Ag⁻¹ current densities, (c) rate performance of the Ce- doped NVP.

$\text{Na}_3\text{V}_{1.96}\text{Ce}_{0.04}(\text{PO}_4)_3$ full cell delivered good discharge capacities 85.7, 83.98, 74.18, 70.91, 65.86, 53.61, and 33.19 mAhg^{-1} at different-different current densities 0.1, 0.2, 0.5, 0.7, 1, 2, and 5 Ag^{-1} , which is higher than NVP material discharge capacities 69.71, 58.16, 50.04, 46.03, 41.94, 34.33, and 23.06 mAhg^{-1} at different-different current densities 0.1, 0.2, 0.5, 0.7, 1, 2, and 5 Ag^{-1} , shown in **Fig 29**. CV profiles for the full cell of the Ce- doped NVP samples at scan rates from 1-10 mVs^{-1} are shown in **Fig.30**.

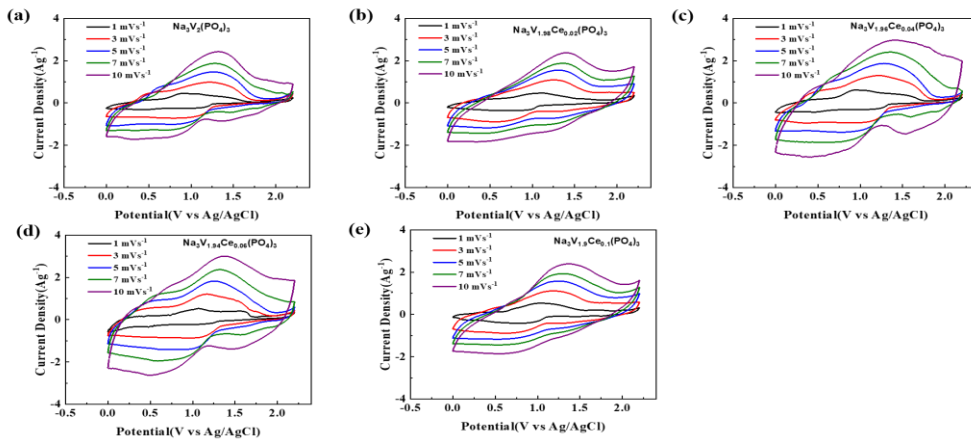


Fig. 30 CV profiles for full cell of the Ce- doped NVP samples at different scan rate.

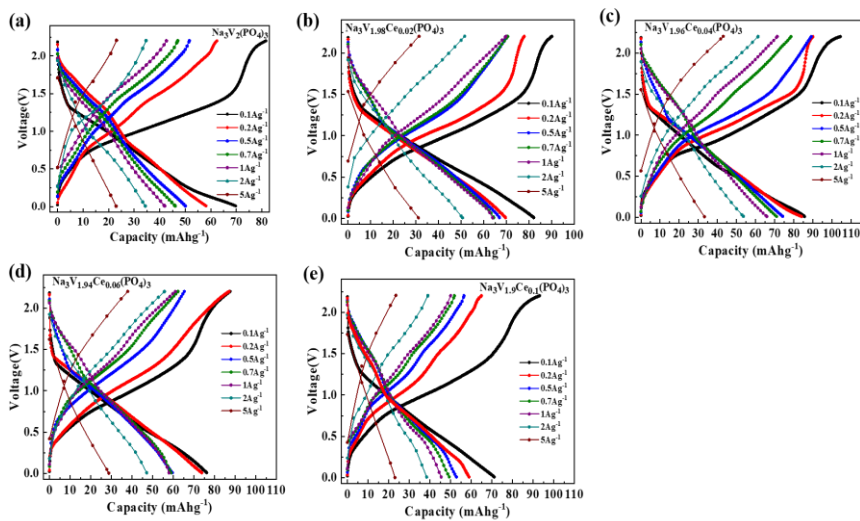


Fig. 31 GCD profiles for the full cell of the Ce- doped NVP samples at different current densities.

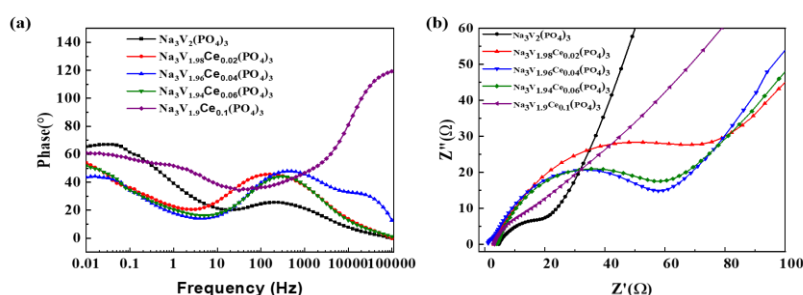


Fig. 32 EIS spectra of the Ce- doped NVP .

Fig. 33 shows the rate performances of the Ce- doped NVP sample along with the C.E at 0.1Ag^{-1} , 0.2Ag^{-1} , 0.5Ag^{-1} , 0.7Ag^{-1} , 1Ag^{-1} , 2Ag^{-1} and 5Ag^{-1} , respectively. For each sample, when current density increasing from 0.1-5 then the discharge-specific capacity decreases in **Fig. 32 (a)** and **Fig. 32 (c)**. In contrast, the C.E in the case of NVP is less than 90%, while that of Ce-doped NVP stays close to 90%, suggesting that Ce-doped material is more stable.

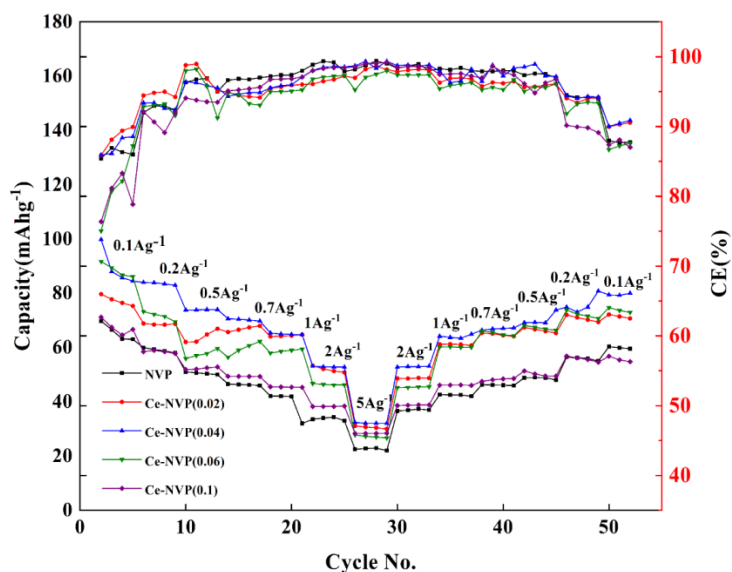


Fig. 33 Rate performance Ce- doped NVP material at 0.1, 0.2,0.5,0.7,1,2,5 Ag^{-1} .

The rate capability of the Ce-4 NVP sample is enhanced within the potential window of 0.01–2.2 V. The discharge-specific capacity of the Ce-4 doped NVP material is 33.19mAhg^{-1} at a current density of 5Ag^{-1} , which is significantly greater than the outcome of the pure NVP. The enhanced sodium ion transport and electron transfer are

primarily responsible for the outcome [22]. The cycling performance of the Ce- doped NVP samples ($x = 0$ and 0.04) at 5 Ag^{-1} in the potential window of 0.01 - 2.2 V is shown in **Fig. 34**.

The Ce- doped NVP ($x = 0$ and 0.04) sample's discharge capacity retentions after 100 cycles are 81.14% and 83.82% , respectively, at 5 Ag^{-1} . The outcome shows that the sample with the best long-term cycle stability is Ce-4 NVP. The exceptional cycling performance may be due to the presence of the inactive Ce-element replacing the Vanadium site, hence acting as a pillar or say support to the NVP crystal structure, and buffering the distortion of NVP pure crystals during charging and discharging together improving the structural stability.

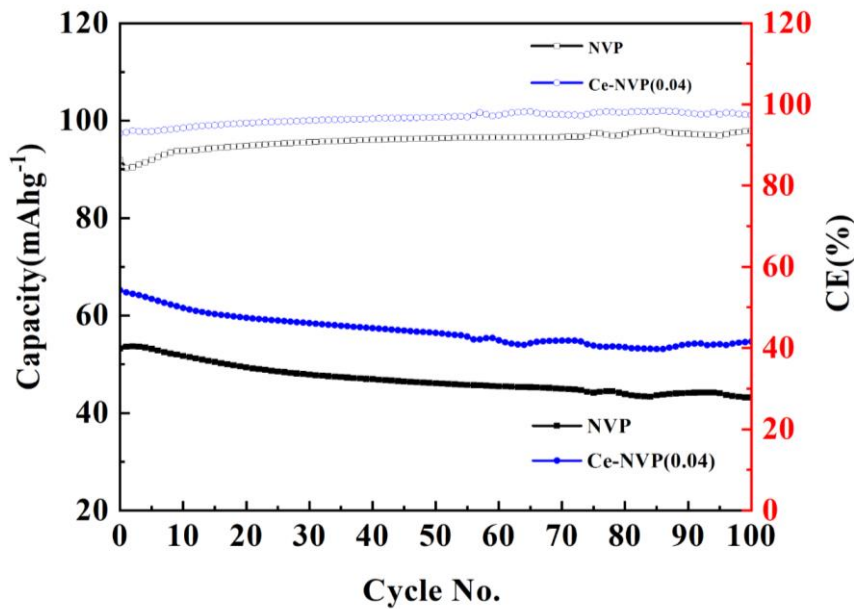


Fig. 34 Cyclic performance of Ce- doped NVP ($x = 0$, and 0.04) material at 5 Ag^{-1} .



Chapter 4

Conclusion and Future Scope

4.1 Conclusion:

In a nutshell, a NASICON-based electrode material was successfully prepared by the rheological phase reaction method. The synthesized NASICON material tends to work as a battery-type electrode. MXene ($\text{Ti}_3\text{C}_2\text{T}_x$) has been used to work as a supercapacitor-type electrode. It is observed that the use of high-concentration electrolytes significantly suppresses vanadium dissolution and enlarges the electrochemical active potential window. The optimized 17m NaClO_4 electrolyte shows a maximum potential window of 3.08V than the low-concentrated 1m NaClO_4 electrolyte 2.72V. Consequently, the side reaction i.e. hydrogen and oxygen evolution is minimized. Also, in the 17m NaClO_4 , pristine NVP electrode shows improved rate capability and specific capacity. In addition, the weak electronic conductivity of pristine NVP is successfully improved by Ce-doping. The structural properties such as phase formation, oxidation state of the elements, surface functional groups, and surface morphology of the as-prepared material were confirmed by various characterization techniques such as P-XRD, SEM, TEM, EDS, FTIR, and RAMAN, respectively. In the full cell configuration ($\text{Na}_3\text{V}_{2-x}\text{Ce}_x(\text{PO}_4)_3//\text{MXene}$), among all the synthesized electrode materials $\text{Na}_3\text{V}_{1.96}\text{Ce}_{0.04}(\text{PO}_4)_3$ exhibits a high specific capacity 85.7mAhg^{-1} specific capacity and maximum energy density of 60.72Wh/kg in 17m NaClO_4 electrolyte. Thus, the utilization of SICs with a highly concentrated electrolyte and highly ionic conductive NASICON electrode system emerges as a favourable method to advance in improving aqueous energy storage devices.

4.2 Future Prospects:

This project work has successfully addressed the development of NASICON-based electrode material for sodium ion supercapacitors. Although this synthesis method for electrode materials is very efficient in terms of cost and easiness, improvement in the conductivity of NASICON material still needs further research. To accomplish this, novel preparation techniques can be investigated like carbon coating, doped metallic elements, etc. It is also essential to accomplish the stability factor in the electrochemical process along with the economical aspect and high performance of electrode materials in SICs. In the proximate future, it is achievable that a supercapacitor device having as good energy density can be presented in the market which is comparable to presently available sodium ion battery systems. Electrochemical supercapacitors are evolving as promising energy storage devices. More research is required to develop high-performance supercapacitor electrodes to meet the growing energy demand and it is also essential to develop further the synthesizing process and parameters also advance the material properties to get extended capability exploration of supercapacitors.

References:

- [1].Najib, S. & Erdem, E. Current progress achieved in novel materials for supercapacitor electrodes: mini review. *Nanoscale Adv.* **1**, 2817–2827 (2019).
- [2].Poonam, Sharma, K., Arora, A. & Tripathi, S. K. Review of supercapacitors: Materials and devices. *J. Energy Storage* **21**, 801–825 (2019).
- [3].Zhou, Q. et al. Sodium Superionic Conductors (NASICON) as Cathode Materials for Sodium-Ion Batteries. *Electrochemical. Energy Rev.* **4**, 793–823 (2021).
- [4].Zhang, L., Liu, Y., You, Y., Vinu, A. & Mai, L. NASICON-type solid-state electrolytes: The history, physicochemical properties, and challenges. *Interdiscip. Mater.* **2**, 91–110 (2023).
- [5].Thirupathi, R., Kumari, V., Chakrabarty, S. & Omar, S. Recent progress and prospects of NASICON framework electrodes for Na-ion batteries. *Prog. Mater. Sci.* **137**, 101128 (2023).
- [6].Ellis, B. L., Makahnouk, W. R. M., Rowan-Weetaluktuk, W. N., Ryan, D. H. & Nazar, L. F. Crystal Structure and Electrochemical Properties of A_2MPO_4F Fluorophosphates ($A = Na, Li$; $M = Fe, Mn, Co, Ni$). *Chem. Mater.* **22**, 1059–1070 (2010).
- [7].Permatasari, F. A., Irham, M. A., Bisri, S. Z. & Iskandar, F. Carbon-Based Quantum Dots for Supercapacitors: Recent Advances and Future Challenges. *Nanomaterials* **11**, 91 (2021).
- [8].Pershaanaa, M., Bashir, S., Ramesh, S. & Ramesh, K. Every bite of Supercap: A brief review on construction and enhancement of supercapacitor. *J. Energy Storage* **50**, 104599 (2022).
- [9].El Aggadi, S., Ennouhi, M., Boutakiout, A. & El Hourch, A. Progress towards efficient phosphate-

- based materials for sodium-ion batteries in electrochemical energy storage. *Ionics* **29**, 2099–2113 (2023).
- [10].Sun, L. et al. Homologous MXene-Derived Electrodes for Potassium-Ion Full Batteries. *Adv. Energy Mater.* **12**, 2200113 (2022).
- [11].Beka, L. G. et al. A 2D metal–organic framework/reduced graphene oxide heterostructure for supercapacitor application. *RSC Adv.* **9**, 36123–36135 (2019).
- [12].Suo, L. et al. “Water-in-Salt” Electrolyte Makes Aqueous Sodium-Ion Battery Safe, Green, and Long-Lasting. *Adv. Energy Mater.* **7**, 1701189 (2017).
- [13].Li, S. et al. The electrochemical exploration of double carbon-wrapped Na₃V₂(PO₄)₃: Towards long-time cycling and superior rate sodium-ion battery cathode. *J. Power Sources* **366**, 249–258 (2017).
- [14].Zheng, Q., Yi, H., Liu, W., Li, X. & Zhang, H. Improving the electrochemical performance of Na₃V₂(PO₄)₃ cathode in sodium ion batteries through Ce/V substitution based on rational design and synthesis optimization. *Electrochimica Acta* **238**, 288–297 (2017).
- [15].Krishnan, S., Gupta, A. K., Singh, M. K., Guha, N. & Rai, D. K. Nitrogen-rich Cu-MOF decorated on reduced graphene oxide nanosheets for hybrid supercapacitor applications with enhanced cycling stability. *Chem. Eng. J.* **435**, 135042 (2022).
- [16].Park, J., Lee, J. & Kim, W. Water-in-Salt Electrolyte Enables Ultrafast Supercapacitors for AC Line Filtering. *ACS Energy Lett.* **6**, 769–777 (2021).

- [17].Huang, Q., Qian, C., Liu, C. & Chen, Y. Simultaneous modification of dual-substitution with CeO₂ coating boosting high performance sodium ion batteries. *J. Colloid Interface Sci.* **654**, 626–638 (2024).
- [18].Chen, P. et al. Ce-doped V₂O₅ microspheres with improved electrochemical performance for high-power rechargeable lithium ion batteries. *J. Alloys Compd.* **784**, 574–583 (2019).
- [19].Phukhrongthung, A. et al. Rocking chair-type aqueous sodium-ion capacitors with biomass-derived activated carbon and Na₃V₂(PO₄)₂F₃ nanoflower in a water-in-salt electrolyte. *J. Energy Storage* **80**, 110369 (2024).
- [20].Liang, Z., Tian, F., Yang, G. & Wang, C. Enabling long-cycling aqueous sodium-ion batteries via Mn dissolution inhibition using sodium ferrocyanide electrolyte additive. *Nat. Commun.* **14**, 3591 (2023).
- [21].Manikandan, R. et al. Vanadium Pentoxide with H₂O, K⁺, and Na⁺ Spacer between Layered Nanostructures for High-Performance Symmetric Electrochemical Capacitors. *Adv. Mater. Interfaces* **5**, 1800041 (2018).
- [22].Song, W. et al. Mechanistic investigation of ion migration in Na₃V₂(PO₄)₂F₃ hybrid-ion batteries. *Phys. Chem. Chem. Phys.* **17**, 159–165 (2015).